AWARD NUMBER: W81XWH-19-1-0199

TITLE: Artificial Intelligence-Based Diffraction Analysis (AIDA) for Point-of-Care Breast Cancer Classification

PRINCIPAL INVESTIGATOR: Dr. Hakho Lee

CONTRACTING ORGANIZATION: MASSACHUSETTS GENERAL HOSPITAL

BOSTON MA 02114-2621

REPORT DATE: July 2020

TYPE OF REPORT: Annual

PREPARED FOR: U.S. Army Medical Research and Materiel Command
Fort Detrick, Maryland 21702-5012

REPORT DOCUMENTATION PAGE

Form Approved
OMB No. 0704-0188

1. REPORT DATE	2. REPORT TYPE	3. DATES COVERED
July 2020	Annual	07/01/2019 - 06/30/2020

4. TITLE AND SUBTITLE

Artificial Intelligence-Based Diffraction Analysis (AIDA) for Point-of-Care Breast Cancer Classification

5a. CONTRACT NUMBER
W81XWH-19-1-0199

5b. GRANT NUMBER

5c. PROGRAM ELEMENT NUMBER

6. AUTHOR(S)
Hakho Lee, PhD

E-Mail: hlee@mgh.harvard.edu

5d. PROJECT NUMBER

5e. TASK NUMBER

5f. WORK UNIT NUMBER

7. PERFORMING ORGANIZATION NAME(S) AND ADDRESS(ES)

MASSACHUSETTS GENERAL HOSPITAL, THE SUSAN ROUDEBUSH
5 FRUIT ST, BOSTON MA 02114-2621

AND ADDRESS(ES)

8. PERFORMING ORGANIZATION REPORT NUMBER

9. SPONSORING / MONITORING AGENCY NAME(S) AND ADDRESS(ES)

U.S. Army Medical Research and Development Command
Fort Detrick, Maryland 21702-5012

10. SPONSOR/MONITOR'S ACRONYM(S)

11. SPONSOR/MONITOR'S REPORT NUMBER(S)

12. DISTRIBUTION / AVAILABILITY STATEMENT

Approved for Public Release; Distribution Unlimited

13. SUPPLEMENTARY NOTES

14. ABSTRACT

The overall goal of this project is to advance a new analytical platform tailor-designed to probe single extracellular vesicles (EVs). Specifically, we will develop a new imaging method to probe individual EVs – the imaging method will use novel cleavable light-tagged antibodies for repeated probing on same EVs. We will next apply this platform to study EVs at very early stages of lung cancers (LCs) using gold standard genetically engineered mouse models of cancer that naturally arise following genetic mutation in the lung tissue, similar to what may occur in humans. We will monitor both tumor burdens and its molecular characteristics; this information will be compared with single-EV profiling results. The study will work backwards from advanced disease towards increasingly minimal disease, with concordant EV analysis and imaging to understand limits of detection.

15. SUBJECT TERMS
breast cancer, holography, deep learning, point-of-care

16. SECURITY CLASSIFICATION OF:			17. LIMITATION OF ABSTRACT	18. NUMBER OF PAGES	19a. NAME OF RESPONSIBLE PERSON USAMRMC
a. REPORT	b. ABSTRACT	c. THIS PAGE			19b. TELEPHONE NUMBER *(include area code)*
Unclassified	Unclassified	Unclassified	Unclassified		

Table of Contents

Page

1. INTRODUCTION

Cellular inspection using microscopy and histology remains integral for diagnosis, prognosis, and treatment decisions. The principal technique, conventional microscopy, has low throughput, requires manual inspection by trained microscopists, and often yields variable, operator-dependent results. Such drawbacks are exacerbated in resource-limited settings where pathology bottlenecks delay cancer diagnoses and potentially lead to over/under-treatment. The problem is relevant not only across low or middle-income countries, but also in the US; nearly a quarter of the US population live in rural areas, but only 10% of physicians practice in those areas8. Developing cost-effective, scalable technologies to feasibly detect (especially at early stages) and classify cancers is thus a key mandate to better manage cancer and improve survivorship. Unfortunately, no such platforms are currently available for translational testing. The ***goal*** of this proposal is to advance a new diagnostic imaging platform for on-site, high-throughput breast cancer cell screening. Termed AIDA (Artificial Intelligence Diffraction Analysis), this platform integrates cutting-edge developments in computational optics and deep learning to facilitate accurate, fast, and automated molecular analyses of breast cancer down to the single cell.

2. KEYWORDS

Breast cancer, Holography, Deep learning, Point-of-care

3. ACCOMPLISHMENTS

What were the major goals of the project?

The major goals of the first-year funding period (2019/07 - 2020/07) were two-fold.

Goal 1: Implement an AIDA platform for large-scale single cell imaging (90% completion, Massachusetts General Hospital).

Goal 2: Develop AIDA deep-learning framework for single cell detection and classification (90% completion, Worcester Polytechnic Institute).

What was accomplished under these goals?

We have made significant progresses in developing both the imaging system and deep learning algorithm.

Massachusetts General Hospital (PI, Hakho Lee)

New AIDA system. We have recently implemented a new whole-slide imaging system for real-time breast biopsy validation (**Fig. 1a**). The system incorporates an on-board embedded GPU (NVIDIA Jetson Nano) for on-site holographic reconstruction without the need to communicate with a cloud-based GPU server (**Fig. 1b**). The GPU's128 cores deliver 450 GFLOPS of computing power which compute holographic reconstruction on images acquired by a 10MP CMOS sensor (Imaging Source) with less than 100 ms of processing latency per acquisition. To complement these enhanced optical and computing modules, we designed a high-precision scanning optical assembly that maintains a constant distance to the sample within 25 μm, and has fine-adjustment mechanisms for tilt, angle, and spatial correction to ensure the highest quality data. Further, the system facilitates automated data acquisition and processing of an entire breast pathology sample (~10^7 cells) using a custom motorized stage. Samples are processed in 7 min; an order of magnitude faster than our previously reported system.

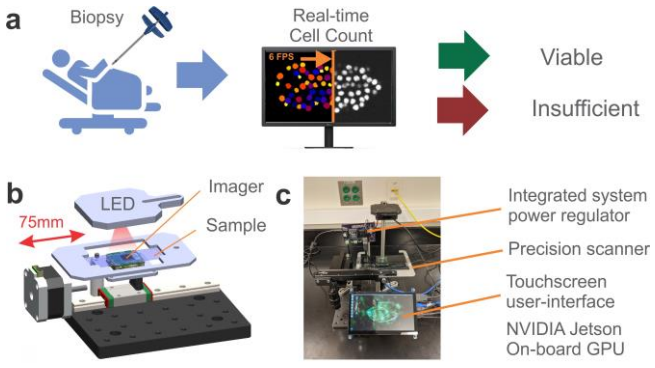

Fig. 1. 2nd generation AIDA system. (a) Updated patient workflow illustrating real-time biopsy validation at the point-of-care **(b)** Precision optical scanning mechanism with 10MP CMOS image sensor **(c)** Photograph of constructed system

Real-time hologram reconstruction. Individual breast cells are holographically reconstructed using a novel deep learning system that is fast and reliable. The system implements fast Fourier transform (FFT)-based two-dimensional image convolutions using the C++ based NVIDIA "CUDA" interface to perform holographic magnitude reconstruction. This pipeline is paired with a custom 5-layer convolutional deep learning

architecture, named HoloNet, in order to accomplish fast and accurate phase recovery. The integrated system can reconstruct holographic image data at a maximum throughput of 15 frames per second on high resolution (2048 × 2048) tiles which are stitched together to yield a field-of-view (FOV) as large as 75 mm × 50 mm: large enough for any pathology application. We are currently implementing graphical, user-friendly software to streamline the system operation using a high definition capacitive touchscreen.

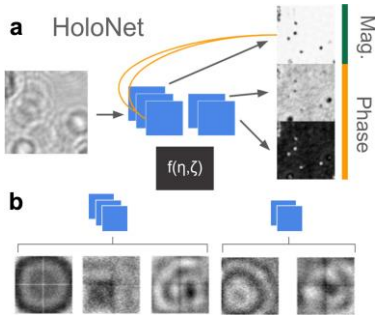

Fig. 2. HoloNet deep learning system. (a) Deep learning pipeline with a sample 192 × 192 input hologram tile. Tile is processed in realtime by five magnitude and phase recovery filters to output a three-channel reconstruction. **(b)** Visualization of the learned filters, demonstrating the machine's ability to learn complex optical transformations.

Worcester Polytechnic Institute (PI, Kwonmoo Lee)

Development of a deep neural network (HoloNet) for the hologram analysis. Using the AIDA system, we obtained high-resolution, large FOV diffraction images that lens-based microscopes cannot achieve. The diffraction images, however, are complicated to discern. There is a computational algorithm that converts the diffraction patterns to cell images, but it is inefficient and prone to errors. To resolve this issue, we developed a deep neural network, called HoloNet, which directly analyzes diffraction patterns (**Fig. 3a**). In addition to the standard CNN (Convolutional Neural Network), the HoloNet includes a holo-branch that extracts large features from holograms and integrate them with the small features from the standard CNN. Since low-level cell features can diffract more than high-level features, the large filters in the holo-branch can effectively capture this information. Using HoloNet, we built a regression model to predict the intensity values of ER/PR and HER2 in breast cancer cell lines. The R^2 values of ER/PR and HER2 regression was 0.9382 and 0.9675, respectively (**Fig. 3b**). We also trained the classifier based on the Holo-Net. The accuracy of the classification for four subtypes of breast cancer was 0.949 (**Fig. 3c**).

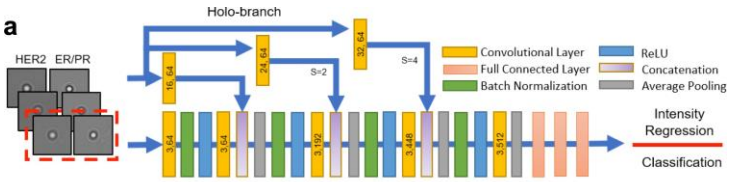

b

Type	R^2	MAE	MSE	RMSE
ER/PR	0.9382	0.0358	0.0028	0.0525
HER2	0.9675	0.0342	0.0029	0.0536

c

Accuracy	F1-Score			
	ER/PR-HER2-	ER/PR-HER2+	ER/PR+HER2+	ER/PR+HER2-
0.949	0.956	0.9701	0.9435	0.9544

Fig. 3. HoloNet analyzes the holograms of breast cancer cells. (**a**) Structure of HoloNet. **(b)** The performances of the regression from ER/PR and HER2 intensities. **(c)** The performances of the classification of breast cancer cell types.

Identification of sub-clusters of breast cancer cells using hologram features. After we trained the classifier, we used the trained HoloNet as a feature extractor from breast cancer cell holograms. We visualized the feature vectors of individual holograms on the three-dimensional space using UMAP (**Fig. 4a**). This revealed that there exist more detailed subtypes within the previously known four breast cancer cell types (**Figs. 4b-e**). To identify the clinical relevance of these sub-clusters, we confirmed that some of these sub-clusters existed in breast cancer patient samples (from the previous study). We used the trained Holo-Net to extract the features from the holograms of two breast cancer patients. In both patients, we found that a substantial amount of the breast cancer cells of Cluster 1, 3, 8, and 9 existed (**Fig. 4f**), suggesting that new clusters may have clinical importance.

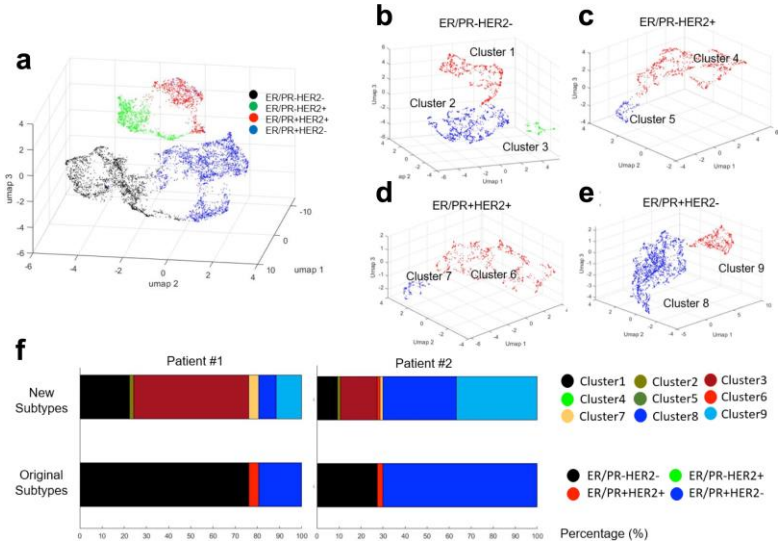

Fig. 4. Sub-clusters of breast cancer cells. (a) Holo-Net-embedded feature distribution of the holograms of breast cancer cells. **(b-e)** Sub-clusters in each breast cancer cell type. **(f)** Distribution of the original molecular phenotypes and new hologram phenotypes from breast cancer patients.

Hologram resolution enhancement. The resolution of the hologram is limited by the pixel size of the image sensor. We tested the feasibility of enhancing hologram resolution using deep learning. We made the original hologram low resolution by 8 pixel averaging (**Fig. 5a**). Then, we trained EDSR to recover the hologram resolution, resulting in increased pixel signal-to-noise ratio (pSNR) and the structural similarity index (SSIM; **Fig. 5b**). The recovered resolution was shown to increase the performance (R^2) of the intensity prediction in each channel in comparison to low resolution hologram (**Fig. 5c**).

a

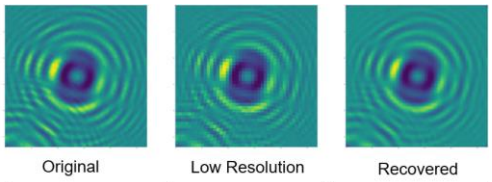

b

	Low Resolution	Recovered Resolution
pSNR (dB)	34.3	39.9
SSIM	0.93	0.98

c

Channel	Original	Low	Recovered
ER/PR	0.9169	0.8747	0.8981
HER2	0.8970	0.6981	0.8129

Fig. 5. Resolution enhancement of hologram. **(a)** Examples of holograms. **(b)** Increased pSNR and SSIM by deep learning-based resolution enhancement. **(c)** R^2 for the intensity prediction using the original, low resolution, recovered resolution holograms

What opportunities for training and professional development has the project provided?

Training activities.

Practical skill sets for optics and computation. [MGH] With the guidance of the PI (H. Lee) and other research fellows, the graduate student (Mr. Ismail Degani, MIT) involved in this project has advanced his skills in low-level GPU programming, optical systems assembly, and data acquisition. Mr. Degani is now conducting this project independently. [WPI] With the guidance of the PI (Dr. Kwonmoo Lee), the graduate students (Mengzhi Cao and Pengyi Ye, Master Students at WPI) involved in this project have advanced their skills on deep learning application to image datasets.

Undergraduate senior design project. [WPI] PI (Dr. Kwonmoo Lee) provided a weekly mentorship to senior undergraduate students (Finn Casey, Robert Farrell, Adam Kaminski, Joseph LeBlanc) for the design project of an AI imaging system for holographic live cell imaging. The students continued to work on the project during Covid-19 pandemic and successfully presented their project on a virtual platform (**Fig. 6**).

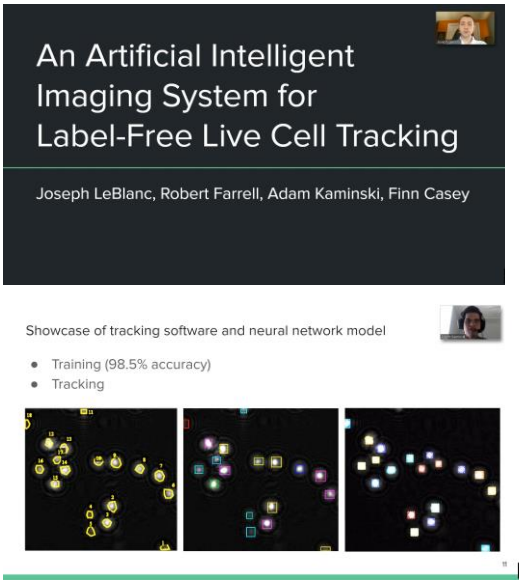

Fig. 6. Virtual presentation of the senior design project during Covid-19 pandemic

Professional development.

Course work. The concepts developed in this project (e.g., hologram, deep learning) has been incorporated into the intramural coursework of *CSB10 – Engineering Biosensors* taught by the PI (H. Lee), that explores key topics in biosensing.

Conference. Mr. Degani was encouraged to present at extramural meetings and conferences (see **Section 6**).

Seminar. The PI (Dr. Kwonmoo Lee) presented the progress of the project at Samsung Genome Institute, University at Buffalo, and Boston Children's Hospital.

How were the results disseminated to communities of interest?

Nothing to Report

What do you plan to do during the next reporting period to accomplish the goals?

[MGH site] As planned in our original Aim 2, we will apply the developed AIDA system to molecularly profile breast cancer cells. We will optimize our staining protocol for ER/PR and HER2. The planned activities will involve a set of controlled titration experiments. Obtained images will be sent to Partnering PI's lab to develop neural networks for image analyses. To ascertain the AIDA's accuracy, the profiling results will be compared with those by gold standard methods (e.g., flow cytometry). In anticipation of the pilot clinical test, we will secure IRB approval at MGH (pending now) and apply for HRPO approval.

[WPI site] *Pixel super-resolution.* To restore subpixel spatial information, we will apply an EDSR deep neural network for super-resolution restoration. We will acquire the training set 1× and 4× magnified diffraction

patterns from the same cells. The network will use these matching image pairs to learn spatial details. The trained network will improve the pixel density of the original diffraction patterns by 16-fold without reducing the field of view. *Generative modeling of cellular details for the fine-grained deconvolution.* To learn the fine-grained features from holograms, we will apply Generative Adversarial Networks (GANs), whose strength is its capacity to learn the cost function, recapitulating fine details in imaging data. The generator of GANs will synthesize reconstructed images of stained cells for given input of diffraction images. The embedded feature vectors of the generator will be used to identify fine-grained clusters, and the molecular markers will be quantified. *AI porting to a microcomputer.* Once algorithm development is complete on a workstation, we will transfer deep neural networks to a local controller for the POC (Point-Of-Care) operation by pruning deep neural network to reduce the model complexity and size for efficient execution. We will use an NVIDIA Jetson TX2 module, which provides deep learning computation in a small form-factor device and offers low power consumption.

4. IMPACT

What was the impact on the development of the principal discipline(s) of the project?

The developed system introduces *a new concept in biosensor design* by combining the advantages of GPU computing advances and lensless holographic imaging. In this improved system, internet connectivity speed and reliability is no longer a limiting factor in the throughput of the system. Rather, the system's self-contained design allows for exceedingly fast and reliable biopsy validation. ***Real-time biopsy validation:*** Our real-time strategy significantly improves the patient workflow by assessing the viability of a biopsy at the point-of-care. This eliminates the possibility of a non-diagnostic sample (having insufficient cell counts) forcing a patient to return for a second biopsy, which in many low-resource settings can be a significant burden. This innovation therefore offers not only higher efficiency but also significantly reduces patient harm. ***Increased spatial and temporal resolution.*** Utilizing the latest semiconductor technology, the imaging sensors can acquire theoretical spatial pixel resolution of 1.1um. This allows the system to resolve very fine details of each cell in the sample biopsy, greatly increasing the accuracy of cell segmentation and classification tasks. ***Novel whole-slide scanning architecture.*** In previous iterations, the system could only image a field-of-view (FOV) of 24mm^2, corresponding to the area of the image sensor. Our new scanning system has increased this *by a factor of 150* to 3750mm^2. This FOV allows imaging of much larger samples which improves the overall versatility of the system. ***Guided optical Calibration.*** Motorized optical systems often need to be extensively calibrated by trained professionals in order to function optimally. Our system by contrast interprets the information-rich holographic image data to readily calculate the system's tilt/axial misalignment. An operator can then easily be guided by the system through the calibration sequences, minimizing the need for labor-intensive, potentially error-prone manual procedures. ***Robustness and user-friendly interface.*** One of the significant merits of the hybrid system is its durability and reproducibility. The system presents simple interfaces for accomplishing all aspects of biopsy validation; users can enjoy the same level of intuitive interfaces which are now standard in consumer electronics.

What was the impact on other disciplines?

Nothing to report.

What was the impact on technology transfer?

Nothing to report.

What was the impact on society beyond science and technology?

Nothing to report.

5. CHANGES/PROBLEMS

Dr. Kwonmoo Lee (PI at WPI) title was changed to Affiliate Assistant Professor on 07/01/2020.

6. PRODUCTS

Publications, conference papers, and presentations

Journal publications.

1. Weissleder, R., and Lee, H. (2020) Automated molecular-image cytometry and analysis in modern oncology. ***Nature Reviews Materials***, 5, 409–422. Acknowledgement of federal support (yes).

Presentations

(All of the following presentations acknowledged the federal support.)

High-throughput protein profiling for cancer diagnostics & prognostic
ISEV-MRS Joint Meeting on EVs in Cancer
Hakho Lee,
Nashville, TN; 02-Aug-2019

Liquid biopsies - overview
SWOG Fall 2019 Group meeting
Hakho Lee
Chicago, IL, 01-Oct-2019

Sample preparation for clinical diagnostics/ Seminar
Korean Institute of Machinery and Materials (KIMM)
Hakho Lee
Seoul, Korea; 10-Oct-2019

Promise of liquid biopsy for cancer management
Applied Pharmaceutical Nanotechnology
Hakho Lee
Cambridge, MA; 25-Oct-2019

Unravelling Cellular and Subcellular Heterogeneity Using Deep Learning
Samsung Genome Institute
Kwomoo Lee
Seoul, Korea; 10-Jan-2020

Unravelling Cellular and Subcellular Heterogeneity Using Deep Learning
University at Buffalo
Kwomoo Lee
Buffalo, NY; 12-Mar-2020

Unravelling Cellular and Subcellular Heterogeneity Using Deep Learning
Boston Children's Hospital
Kwomoo Lee
Boston,MA; 12-Mar-2020

Technologies or techniques.
The research has produced a library of procedures to make optical systems, fluidic devices, and bioconjugtation (antibodies). We also advanced new neural network algorithms to rapidly analyze holograms. All data will be electronically stored and archived, and will be made available through publications in peer reviewed journals. As in the past, all of these resources will be shared freely with scientific community upon execution of a proper MTA through the Office of Corporate Licensing (MGH or WPI).

Other products
Nothing to report.

7. PARTICIPANTS & OTHER COLLABORATING ORGANIZATIONS

What individuals have worked on the project?

Name:	*Hakho Lee (MGH)*
Project Role:	*Principal Investigator*
Researcher Identifier	*orcid.org/0000-0002-0087-0909*
Nearest person month worked:	*2*
Contribution to Project:	*Dr. Lee supervised the overall research, interacting with investigators and research fellows, and discussing all experimental designs and data.*
Funding Support:	

Name:	*Cesar M. Castro (MGH)*
Project Role:	*Co-Investigator*
Researcher Identifier	*N/A*
Nearest person month worked:	*1*
Contribution to Project:	*Dr. Castro guided the biological research, identifying biomarkers for breast cancer detection, and validating the selection through in-vitro assays.*
Funding Support:	

Name:	*Michelle Specht (MGH)*
Project Role:	*Ci-Investigator*
Researcher Identifier	*N/A*
Nearest person month worked:	*1*
Contribution to Project:	*Dr. Specht provided translational guidance for the development of proposed imaging technology. She will help procure breast cancer specimens for diagnostic testing.*
Funding Support:	

Name:	*Ismail Degani (MGH)*
Project Role:	*Graduate student*
Researcher Identifier	*N/A*
Nearest person month worked:	*6*
Contribution to Project:	*Mr. Degani designed the holographic imaging system, constructed the deep learning framework for cell classification/segmentation, and validated the entire system.*
Funding Support:	

Name:	*Kwonmoo Lee (WPI)*
Project Role:	*Principal Investigator*
Researcher Identifier	*orcid.org/0000-0001-6838-7094*
Nearest person month worked:	*1*
Contribution to Project:	*Dr. Lee supervised the overall research, interacting with investigators and research fellows, and discussing all computational analysis results.*
Funding Support:	

Name:	*Tzu-Hsi Song (WPI)*
Project Role:	*Postdoctoral fellow*
Researcher Identifier	*N/A*
Nearest person month worked:	*4*
Contribution to Project:	*Dr.Song designed the holographic deep learning structure (Holo-Net), and perform the unsupervised learning using holograms.*
Funding Support:	

Name:	*Pengyi Ye (WPI)*
Project Role:	*Graduate student*
Researcher Identifier	*N/A*

Nearest person month worked:	*4*
Contribution to Project:	*Mr. Ye performed deep learning-based super-resolution restoration of holograms*
Funding Support:	

Name:	*Mengzhi Cao (WPI)*
Project Role:	*Graduate student*
Researcher Identifier	*N/A*
Nearest person month worked:	*4*
Contribution to Project:	*Mr. Cao performed deep learning-based regression analysis to predict the molecular marker intensities*
Funding Support:	

Has there been a change in the active other support of the PD/PI(s) or senior/key personnel since the last reporting period?

New support (Kwonmoo Lee)

Title:	Unraveling subcellular heterogeneity of molecular coordination by machine learning
Goals:	The major goal of this project is to develop a novel machine learning framework for large-scale analyses of subcellular heterogeneity of cell protrusion.
Specific Aims:	1) Deconvolution of subcellular heterogeneity of protrusion and molecular coordination in live cells 2) Deep learning based high-throughput fluorescence live cell imaging 3) Mechanosensitivity of subcellular bioenergetic status in cell protrusion
Start Date:	15-Sep-2019
End Date:	31-Aug-2024
Level of Effort:	2 Summer Months, 13.334%
Level of Funding:	$1,738,826.00
Funding Agency:	National Institutes of Health/NIGMS
Contracting/Grants Officer:	Dr. Paul Sammak, sammakpj@nigms.nih.gov, 301-594-8494
Role on Project:	Principal Investigator
Overlap:	None. This project is focused on developing a machine learning method applied to fluorescence live cell images to characterize actin regulator dynamics in cell migration. The machine learning method proposed here is focused on noisy fluorescence movies and time series data, which are substantially different from those in the DoD project. The application area is basic cell biology which is also different from breast cancer diagnosis in the DoD project. This project overlaps with the above pending NIH R01 project, but not with the DoD project.

Expired support (Kwonmoo Lee)

Title:	Wearable Devices for In-Home Monitoring of Patients at Risk for Heart Failure
Goals:	The major goal of this project is to develop a novel device for in-home monitoring of heart failure patients who are at risk of developing acute decompensated heart failure.
Specific Aims:	1) Develop reuseable carbon-black and polydimethylsiloxane (CB/PDMS) electrodes that capture bioimpedance and electrocardiogram data 2) Develop hardware and algorithms for acute decompensated heart failure detection, resulting in a wearable monitor with embedded CB/PDMS electrodes 3) Develop hardware and algorithms for atrial fibrillation detection using a smart watch 4) evaluate the performance and usability of both detection systems in a prospectively recruited cohort study.
Start Date:	01-Oct-2015

End Date:	30-Sep-2019
Level of Effort:	0 Calendar month, 0.0%
Level of Funding:	$32,593.00
Funding Agency:	National Science Foundation
Contracting/Grants Officer:	Dr. Wendy Nilsen, wnilsen@nsf.gov, (703) 292-2568
Role on Project:	Co-Principal Investigator
Overlap:	None

What other organizations were involved as partners?
Nothing to report.

8. SPECIAL REPORTING REQUIREMENTS

Not applicable.

9. APPENDICES

The following papers are attached.

Weissleder, R., and Lee, H. (2020) Automated molecular-image cytometry and analysis in modern oncology. ***Nature Reviews Materials***, 5, 409–422. Acknowledgement of federal support (yes).

Automated molecular-image cytometry and analysis in modern oncology

Ralph Weissleder[1,2,3] ✉ *and Hakho Lee*[1,2]

Abstract | Diagnostic methods for initial diagnosis and patient stratification for treatment are key to modern oncology, but many challenges remain. In developed countries, advances in early diagnosis and therapeutics have led to challenges in the sampling of sub-centimetre lesions, with repeat biopsies straining accuracy and throughput of pathological assessment. Conversely, low-income and middle-income countries face extremely limited pathology and imaging resources, large caseloads, convoluted and inefficient workflows, and a lack of specialists. Advances in material sciences, chemistry, engineering and artificial intelligence have led to the introduction of a new class of affordable image cytometers that enable automated cell phenotyping, with ongoing clinical testing indicating that these systems can alleviate existing bottlenecks and improve diagnostic efficiency. Ultimately, these diagnostic methods are likely to surpass current pathology approaches on the basis of the richness of molecular measurements and the fact that they require only scant cellular material, rather than tissue sections. As these methods can be miniaturized and are low-power, they can also be used in point-of-care settings. In this Review, we focus on new devices and approaches for the integrated analysis of scant cancer samples, particularly those obtained by fine-needle aspiration.

Cell-based cancer diagnostics are essential for clinical decision-making, particularly for establishing the correct diagnosis, choosing the appropriate treatment, enrolling patients in clinical trials, assessing therapeutic efficacy and/or restaging disease[1]. In current clinical practice, cancer specimens are commonly obtained by image-guided biopsy, fine-needle aspiration (FNA), surgical-tissue harvesting, punch biopsies, brushings, swabs, biopsy touch preparations ('touch preps'), fluid aspiration or blood analyses. Some of these methods (for example, core biopsies and open surgical biopsies for histopathology) yield abundant tissue for sectioning and staining, whereas other approaches (for example, brushings and touch preps for cytopathology) yield scant amounts of cellular materials. FNA can often be obtained with minimal intervention using small-gauge needles (20–25G), have very low complication rates and are generally well tolerated[2].

Rapid on-site assessment of cellular specimens has become increasingly important to narrowing the time between intervention and initiation of therapy, assuring specimen quality for subsequent diagnoses and minimizing sample degradation and loss during transport. The current workflows are still labour-intensive and are often centralized, requiring extensive sample processing and expert cytopathology review. Digital cytopathology and whole-slide imaging[3] have been implemented, but they also require substantial time, labour and financial investment. Taken together, these factors limit the throughput, financial affordability and global reach of cell-based cancer diagnostics.

A particular challenge to the implementation of cell-based cancer diagnostics is the reliable analysis of scant cellular specimens, either through manual imaging (which requires a trained cytopathologist to review an entire slide) or automated analysis (which incorporates machine-learning routines for automated analysis). Driven by advances in materials science, chemistry, engineering and artificial intelligence (AI), a new class of cell-based cancer diagnostics is emerging to address this challenge. In this Review, we discuss this new generation of automated molecular-image cytometers that uses advanced materials, engineering and AI approaches for digital cell phenotyping. These new 'all-in-one' systems address a potentially large unmet clinical need by enabling advanced cellular diagnostics and are well suited to: meeting the demands of an underserved global healthcare market; repeat sampling at ultra-low invasiveness through the use of small-gauge needles (which can reduce morbidity and is important in clinical trials where frequent sampling is desirable); improving turnaround times through point-of-care analysis and by avoiding biopsy core processing; improving and automating quality control; and reducing both time-to-diagnosis

[1]*Center for Systems Biology, Massachusetts General Hospital, Boston, MA, USA.*

[2]*Department of Radiology, Massachusetts General Hospital, Boston, MA, USA.*

[3]*Department of Systems Biology, Harvard Medical School, Boston, MA, USA.*

✉*e-mail: ralph_weissleder@hms.harvard.edu*

https://doi.org/10.1038/s41578-020-0180-6

and the variability of interpretation through automation. These emerging technologies complement others that are not covered in this Review, namely, low-cost flow cytometers[4,5], liquid biopsies focusing on cell-free DNA (cfDNA)[6], exosomes[7] and circulating tumour cells (CTCs)[8–10], and genomic screening tools (such as the FoundationOne companion diagnostic (F1CDx) and the next-generation-sequencing-based MSK-IMPACT diagnostic assay)[11–13]. Herein, we focus on the automated analysis of cellular specimens obtained by FNA (FIG. 1) and highlight the stains, affinity ligands and biomarkers required for molecular diagnosis, optical technologies used for image cytometry and machine-learning algorithms for automated image analyses, providing relevant examples of clinical applicability. Finally, we offer our perspectives on the current state of the field and on future developments.

Stains and biomarkers

Important considerations for the automated analysis of cellular specimens include chromogenic cellular stains, labelled antibodies for immunostaining and cycling technologies. Each of these staining approaches has to be optimized and the choice of biomarkers validated.

Generic cellular stains. Conventional cytopathology largely relies on chromogenic stains such as haematoxylin and eosin (H&E), Papanicolaou (Pap) and Giemsa. Stained specimens are reviewed by cytopathologists, who evaluate cells for a number of parameters, such as the nuclear:cytoplasmic ratio, nuclear features, mitoses, cell clusters, cell uniformity and cell cohesiveness[14–16]. Such analyses can be automated but are inherently limited by the lack of molecular information, resulting in variable diagnostic accuracies[17]. Most commercial cell analysers (TABLE 1) use this chromogenic staining approach for the automated analysis of white blood cells, whose morphometric features are much more homogenous than those of highly variable cancer cells[18,19].

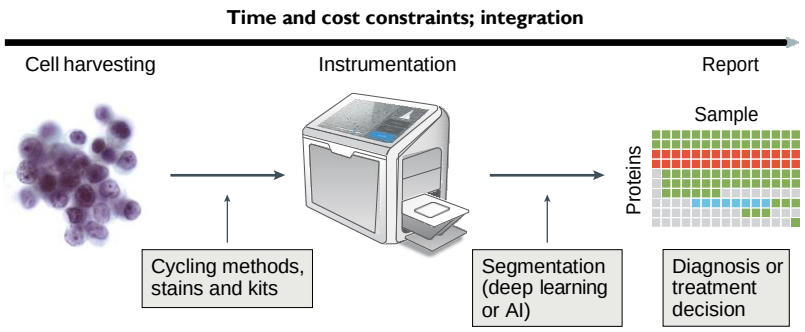

Fig. 1 | **Overview of automated molecular-image cytometry.** Small numbers of cancer cells obtained by fine-needle aspiration, brush biopsies (brushings), biopsy touch preparations (touch preps) or sampling of blood and/or bodily fluids can be subsequently analysed using automated molecular-image cytometry. Cycling methods, instrumentation and computational approaches are essential to the integrated and automated processing of such cells. Indeed, the analysis relies heavily on deep-learning and artificial intelligence (AI) approaches to extract information from dozens of channels and convert them into information that can inform patient management, including diagnosis and treatment decisions. For point-of-care settings, all of the above must occur within reasonable time frames and at a low cost.

Alternative dyes for the investigation of nuclear morphological features (such as aneuploidy and segmentation) include 4′,6-diamidino-2-phenylindole (DAPI), acridine orange, ethidium iodide, propidium iodide or flavins[20]. However, given the limitations of generic chromogenic staining, immunostaining for cancer-associated and host-cell markers has emerged as an alternative and is widely used for CTC analysis.

Immunostaining. Antibodies are increasingly being used in cytopathology, with the standard method being to perform one stain at a time, primarily using immunocytology (which involves absorption measurements of chemical reactions catalysed by antibody-conjugated enzymes) rather than immunofluorescence (which involves emission measurements of fluorescently labelled antibodies). This approach is a practical choice for the detection of key molecular cancer biomarkers while also enabling morphological assessment of cancer cells; for example, human epidermal growth factor receptor 2 (HER2) immunostaining in H&E slides enables simultaneous molecular and morphological assessment.

Multichannel fluorescence imaging allows the interrogation of molecular markers in cells via fluorescently labelled antibodies, typically in 4–8 channels. To further increase the number of biomarkers that can be analysed per cell (>20 channels), cycling technologies have been developed. These methods allow repeatedly staining, destaining (quenching) and restaining of cancer tissues. This, in turn, improves the depth of cell-by-cell profiling, pathway analysis and immunoprofiling in scant FNA samples. To compare different cycling methods[21–24], it is useful to consider how much of the sample is destroyed and/or lost during repeated washing and often harsh quenching conditions, how fast the quenching step is (which often ranges from tens of minutes to hours) and how fast each staining step is. Most cycling methods were originally developed for paraffin-embedded tissue sections that can withstand harsh destaining conditions. Unfortunately, however, these harsh conditions, which require the use of oxidants for bleaching, are often incompatible with FNA samples because the already scant cells are destroyed or lost during washes. Furthermore, it was not uncommon for early cycling technologies to require days to process samples.

Several cell-compatible cycling technologies have been developed over the past 5 years (FIG. 2; TABLE 2). We initially devised and validated multiple DNA-barcoded antibody technologies, including antibody barcoding with photocleavable DNA (ABCD)[25,26] and single-cell analysis for tumour phenotyping (SCANT)[24], while other groups have experimented with amplification strategies[27]. Although the SCANT method was shown to be robust and useful for pathway analysis in a clinical setting[24], one of the obstacles with this method was its comparatively modest signal-to-noise ratio and the long destaining times (0.5–1 h). The fast analytical screening technique (FAST), the latest method, bypasses these shortcomings and enables extremely fast cycling (>95% quenching in <10 s) (FIG. 2).

Table 1 | **Overview of experimental and commercial cell analysers**

Name	Imaging modality	Multiplex[a]	Cost[b]	Application	Ref. or company
Experimental prototypes					
D3	Holography	1	$	FNA samples	[45]
CEM	Holography	<3	$	Cancer FNA samples	[32]
AIDA	Holography	<3	$	Cancer FNA samples	[31]
CytoPAN	Fluorescence	4–6 (up to 20–40 with cycling)	$$	Cancer FNA samples	Under development
FPM	RGB	<3	$$	Tissue section	[59]
Commercial systems					
ThinPrep	RGB	<3	$$$$	Cervical (Pap) smear	Hologic
FocalPoint GS	RGB	<3	$$$$	Cervical (Pap) smear	Becton Dickinson
BestCyte	RGB	<3	$$$$	Cervical (Pap) smear	CellSolutions
CellaVision	RGB	<3	$$$$	WBC analysis	CellaVision
miLab	RGB, fluorescence	<3	$$$	WBC analysis	Noul
Iris	RGB	<3	$$$$	Urine analysis	Beckman Coulter

FNA, fine-needle aspiration; Pap, Papanicolaou; RGB, red, green and blue light; WBC, white blood cell. [a]Refers to the number of stains and not extractable image features. [b]Estimated cost of an instrument: $, <US$1,000; $$, US$1,000–US$4,999; $$$, US$5,000–US$9,999; $$$$≥US$10,000.

Choice of biomarkers. Selecting appropriate molecular markers is essential for identifying cancer cells, differentiating them from non-transformed host cells and profiling a growing number of treatment-relevant immune cells. Although host-cell markers have been thoroughly characterized by extensive flow-cytometry studies, epithelial cancer markers are more diverse and, therefore, require more immunostains for reliable detection. Furthermore, cancer markers are typically only expressed in a fraction of cells and patients. Although much more work needs to be done in this field to refine the choice of biomarker, a number of marker combinations have had some success in identifying cancer cells and differentiating them from host cells. Prominent examples include: epithelial cell adhesion molecule (EpCAM), cytokeratins, CD45 and CD16 for the identification of CTCs[28]; four-marker combination (the 'quad' marker set) comprising epidermal growth factor receptor (EGFR)+ EpCAM + mucin 1 (MUC1)+ WNT2 or EGFR, EpCAM, HER2 and MUC1[29,30]; HER2, oestrogen receptor (ER)/progesterone receptor (PR) for breast cancer[31]; CD19, CD20, immunoglobulin-κ and immunoglobulin-λ light chains and the proliferation marker Ki67 for lymphoma[32]; EGFR, thyroid transcription factor 1 (TTF1; also known as NKX2-1), chromogranin and synaptophysin for lung cancer[33]; EpCAM, calretinin, CD45 and vimentin (the 'ATCdx' marker set) for ovarian cancer[34]; and markers for mutated proteins, such as KRAS-G12D, EGFRv3, IDH1-R132G and BRAF-V600E, among others. This list is clearly not exhaustive but rather represents what has, to date, been used in automated cell analysers. We expect that the number of specific biomarker combinations and better immunostains (antibodies) and will grow in the future.

Optimizing materials for cellular analysis. Freshly obtained clinical samples need to be fixed, stained and captured on glass before they can be analysed. All of these steps require careful optimization and, often, modified materials. Fixation can usually be done in paraformaldehyde, methanol, propanol or other commercially available mixes, such as CytoRich Red (CRR). We have found empirically that some FNA samples of solid neoplasm are preserved better in 50%-diluted CRR, whereas fixation duration (ideally 15–30 min) is less critical.

Immunostaining is best performed in small plastic vials by adding antibody reagents to cells in a staining buffer. Antibody–fluorochrome stability, quality-control issues and limited access to basic tools (for example, centrifuge filters) are notable hurdles when using immunostains in remote areas and in point-of-care devices. The use of lyophilized antibodies and 'cocktails' that contain all of the necessary reagents can reduce variability[35].

An alternative immunostaining approach is to stain cells directly on glass slides after capture. Capturing cells on a glass slide is also critical to ensure that cells can be brought to the focal plane. Capture can be done using biological 'glues' (such as dopamine, biotin and neutravidin or polylysines) as slide coatings or, alternatively, glass slides can be coated with capture antibodies. Irrespective of the method used, careful validation is required for different applications. Non-specific antibody binding can often be reduced by coating slides with blocking materials such as bovine serum albumin (BSA) or polyethylene glycol (PEG) polymers.

To simplify sample handling and processing, commercial systems will likely adapt cartridges to perform all of the above steps in a single platform. One such example is in the miLab system (Noul), which incorporates cellular processing and staining in a single cartridge.

Image-cytometry systems

To inspect heterogeneous cell populations with statistical confidence, image cytometers must visualize large numbers of individual cells. Conventional geometric optics, however, are inherently constrained by the so-called space–bandwidth product (SBP)[36] and, therefore,

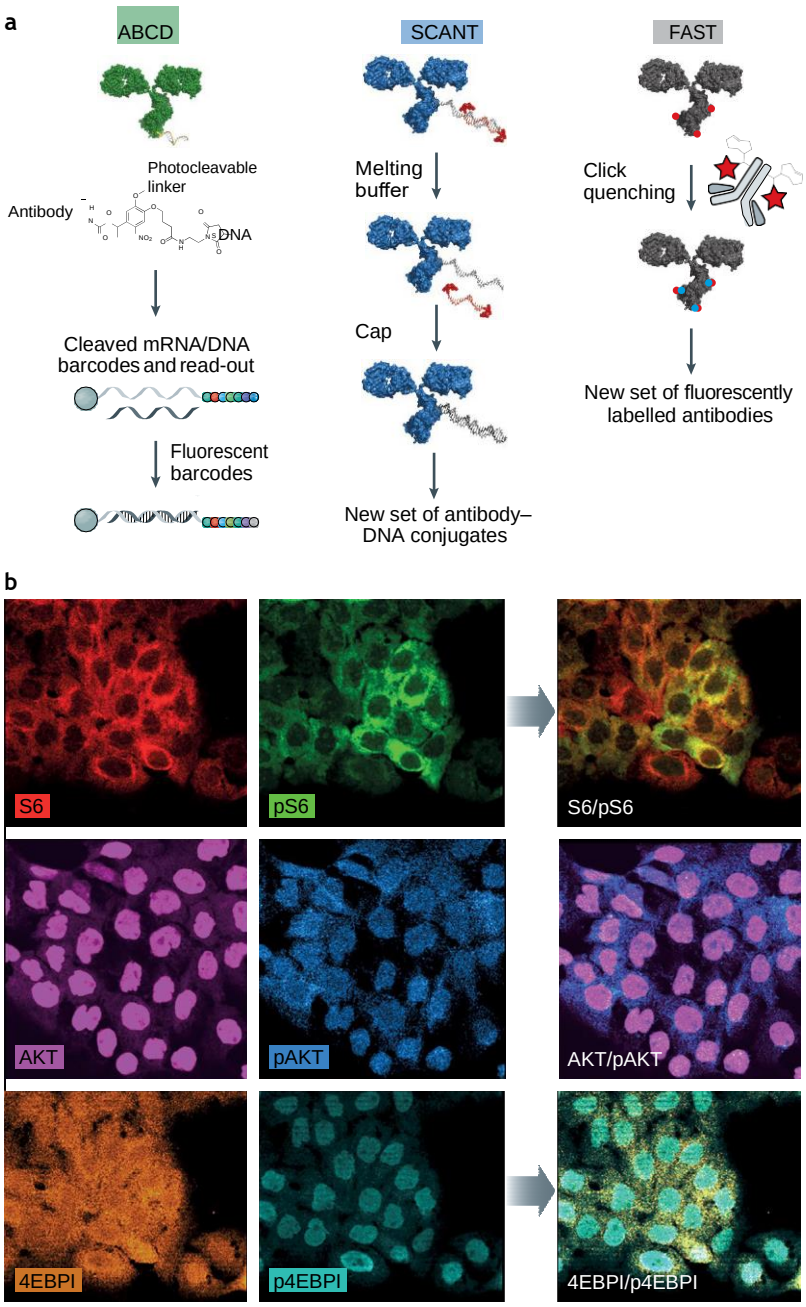

Fig. 2 | **Cyclic labelling technologies for multiplexed cancer-marker and host-cell-marker assessment. a** | An overview of the different cycling techniques, including antibody barcoding with photocleavable DNA (ABCD), single-cell analysis for tumour phenotyping (SCANT)[24] and fast analytical screening technique (FAST), is shown. In ABCD, DNA-barcoded antibodies bound to tissue of interest are photocleaved and then digitally detected by fluorescent barcodes or sequencing[25]. In SCANT, the primary barcoding stand on an antibody of interest contains a complementary imaging strand consisting of 13 bp and two fluorochromes. After imaging, the fluorescent strands are simply washed off with melting buffer and the primary strands are capped to reduce additional cycle-to-cycle background. Both ABCD and SCANT require several hours for processing. In FAST, fluorescently labelled antibodies are quenched with custom-designed clickable quenchers (<10 s), allowing multichannel imaging of 20–30 markers within an hour. **b** | Example of multiplexed single-cell profiling using the SCANT technique. Here, SCANT was applied to profile phosphoproteins in human A431 epidermoid carcinoma cells. Representative examples of phosphoprotein ratio imaging for ribosomal protein S6 (S6)/pS6RP, RACα serine/threonine-protein kinase (AKT)/pAKT and eukaryotic translation initiation factor 4E-binding protein 1 (4EBP1)/p4EBP1 are shown. Panel **b** is adapted from REF.[24], CC-BY-4.0 (https://creativecommons.org/licenses/by/4.0/).

produce megapixel information. This translates to a familiar experience — common microscopes have either a wide field of view (FOV) at low resolution or a small FOV at high spatial resolution, but not both at the same time.

Most laboratory imaging systems overcome this limit by combining high-magnification optics with mechanical stages to automatically scan slides and then transmit the information. Whole-slide imaging and digital-cytopathology technologies have progressed over the years[37] but challenges remain. Two key issues in digital cytopathology are focusing and the need for expert review. The focusing issue has largely been solved via either autofocusing algorithms or 3D imaging of thick *z*-stacks. Autofocusing software often uses either a least-squared or a mean-value method to locate the ideal focus plane[3], whereas 3D imaging, such as microscopy with optical sectioning, requires confocal laser scanning microscopy (CLSM), two-photon microscopy, structured illumination microscopy (SIM), light-sheet fluorescence microscopy (LSFM) or inverted selective plane illumination microscopy (iSPIM)[38]. All of these methods require expensive instrumentation and expert users, and often generate very large data sets[3,38,39]. As such, this particular approach limits deployment in resource-constrained remote locations.

New technological advances are increasingly enabling automated molecular-image cytometry, which is particularly helpful for point-of-care use. Computational optics, wherein optically encoded images are digitally interpreted, can expand the SBP beyond the physical limit of the optics. Advances in optoelectronics and micro-optics further enable the construction of compact, easy-to-control, high-performance systems. Using these approaches can also decrease the overall system cost, as optoelectronic parts and computation have become inexpensive. Three emerging modalities embody these new concepts — digital-holography cytometry, Fourier-ptychography cytometry and miniaturized-fluorescence cytometry.

Digital-holographic cytometry. Holographic imaging is coherent bright-field imaging that records an interference pattern or a hologram between a reference beam and an object. Digital holography acquires such holograms in a digital format and computationally converts them into object images. This approach can greatly simplify optics, as a light source, usually a light-emitting diode (LED), imaging objects and a digital imager can be aligned along the same optical axis[31,32,40–45] (FIG. 3a). This configuration, called lens-free digital in-line holography (LDIH), renders the system compact and cost-effective, requiring no intermediate optical components such as lenses and filter sets. By placing the samples directly on top of an imager, LDIH achieves a large FOV, equivalent to the entire sensing area of the imager (FIG. 3b). High spatial resolution is obtained through numerical image reconstruction (FIG. 3c), particularly using iterative phase-retrieval processes[32]. Reconstructed holograms, therefore, contain a greater amount of information (~10^8 pixels) than a conventional microscope of similar spatial resolution (~10^6 pixels). Furthermore, as LDIH

Table 2 | **Comparison of cellular cycling techniques**

Technique[a]	Targets	Channels	Cycles	Time	Cost[b]	Refs
ABCD; bead-based, fluorescent barcodes	<100	NA	NA	>1 day	$$$	25,26
SCANT; DNA–fluorochrome hybridization	~20–30	4–6	4–5	1 day	$$	24
FAST; site-specific, instant quenching	~20–40	4–6	6–8	<1 hour (for 20 markers)	$	NA

ABCD, antibody barcoding with photocleavable DNA; FAST, fast analytical screening technique; NA, not applicable; SCANT, single-cell analysis for tumour phenotyping. [a]Collectively, these cycling technologies enable the imaging of 20–40 targets in individual cells and can be used for cellular mapping, cellular pathway analysis or heterogeneity studies. [b]Estimated reagent cost for a single sample imaged at 20–100 channels: $, <US$50; $$, US$50–US$499; $$$, <US$500–US$4,999.

is a quantitative phase-imaging technique[46], phase information can be used to infer cell morphology and intracellular content related to the refractive index[47].

Various LDIH systems have been developed. Highly portable systems were initially designed based on smartphones[45], using phone-embedded cameras as detectors. Stand-alone devices were subsequently developed for global health applications, incorporating additional user-friendly features (including touchscreens and sample cartridges) that are difficult to integrate into smartphones[32] (FIG. 3d). Initial LDIH applications typically identified biological targets (such as blood cells, bacteria and *Caenorhabditis elegans*) on the basis of their unique morphology[40,48–50]. Over the past 5 years, new labelling strategies have been explored to impart molecular specificity, thereby improving diagnostic accuracy. In one example involving the labelling of cells with molecularly specific microbeads to alter holographic patterns (FIG. 3c), counting the number of cell-bound beads enabled quantitative molecular profiling of cancer cells[45]. Immunocolour staining is another approach to molecular profiling (FIG. 3e), as hologram intensities (light absorbance) can vary according to staining levels. This approach has been exploited for breast-cancer phenotyping in point-of-care settings[31]. Measurements of molecular biomarker expression using these methods are generally concordant with flow-cytometry-based measurements (FIG. 3f).

However, despite its promise, technical challenges remain for on-site LDIH applications. Hologram reconstruction is a computationally intensive process that requires a powerful computer, preferably one equipped with graphical processing units (GPUs), or cloud computing with a reliable network connection. Deep-learning-based machine vision might mitigate some of these requirements[32,51,52] (FIG. 3g), but its robust performance across a broad range of samples has yet to be demonstrated. Furthermore, spatially connected or dense biological objects can be difficult to image using LDIH, as the numerical phase retrieval becomes unstable. In such samples, multiple measurements with different physical parameters — such as sample-to-sensor distances[53], illumination angles[54] and wavelengths[31,55] — are necessary. LDIH also has limited multiplexing capacity; immunobead labelling is best suited to single-marker or dual-marker detection per sample and colour staining for ≤3 markers in the same sample. Thus, diagnostics based on cellular morphology and a few molecular markers would be a niche application for LDIH.

Fourier-ptychography cytometry. In Fourier ptychography, a set of overlapping, spatially shifted diffraction patterns are acquired and then numerically stitched (or 'folded', hence, the Greek prefix ptychí) to generate a larger diffraction pattern. The strategy effectively increases the numerical aperture (NA) of an optical system, improving spatial resolution without compromising the FOV[31,55]. Most Fourier ptychography microscopy (FPM) systems use programmable LED arrays as an illumination source, and data acquisition starts with taking a sequence of wide-FOV images at low magnification by changing the illumination pattern of the LED array (FIG. 4a). Individual images have low resolution and contain a spatially shifted spectrum of an imaged sample in the Fourier domain (FIG. 4b). Numerical post-processing coherently combines these intensity-only images in the Fourier space to recover high-frequency information. Through this process, the numerical aperture (NA_{FPM}) of the system becomes the sum of NA values of an objective lens (NA_{obj}) and an illumination source (NA_{light})[56]. Thus, for a given incident light (wavelength λ), FPM can achieve a higher resolving power ($\sim\lambda/(NA_{obj}+NA_{light})$) than a regular microscope ($\sim\lambda/NA_{obj}$). FPM yields gigapixel-level information, enabling high-resolution imaging of numerous cells, and can even reveal subcellular detail[57] (FIG. 4c). Furthermore, using low magnification objectives, FPM also supports a large focal depth, robust to variations in sample thickness.

Technical developments over the past 5 years have advanced FPM systems closer to point-of-care use. The original FPM method was time-consuming and resource-intensive, as large numbers (>200) of raw images were acquired by sequentially turning on a single LED. A new illumination scheme has increased the speed of this process through the use of a pseudorandom illumination pattern designed to minimize data redundancy in the Fourier space[57], acquiring fewer images (~40). Furthermore, a deep-learning approach to Fourier-spectrum recovery can ease the computational load of image processing[58]. Fundamental drawbacks, however, remain. For example, the aforementioned multiplexing challenges that limit LDIH still apply because FPM is a form of coherent-light microscopy. FPM also requires thin samples with a smoothly varying phase; this is necessary to map the low-resolution images, obtained at different incident angles, to different passbands of the Fourier spectrum and to, thereby, recover a high-resolution sample image[59–61].

Miniaturized-fluorescence cytometry. As the list of known cancer biomarkers grows, the need for multiplexed cellular profiling also increases, largely driven by interest in improving diagnostic accuracy and facilitating molecularly based treatment decisions. Conventional immunocytology, which is based on chromogenic staining and bright-field microscopy, typically probes only for a few biomarkers simultaneously. Fluorescent imaging, particularly in combination

with cycling technologies, is a potent approach for in-depth multiplexing; a major technical challenge is to transform bulky, expensive microscopes into compact, affordable equivalents for point-of-care use. Fortunately, advances in optoelectronics have made high-quality miniaturized optical parts available, prompting new systems engineering. For example, small LEDs can deliver sufficient power to replace conventional lamps or lasers as an excitation light source, and the photosensitivity of semiconductor imagers has improved substantially for reliable low-light detection[62]. Another opportunity is to augment manual image curation with automated analyses using machine-learning approaches.

Thumb-sized fluorescent microscopes (miniscopes) integrate optical components into a single device[62] (FIG. 5a). Using a gradient-refractive-index objective lens enables shortening of the optical path and can drastically

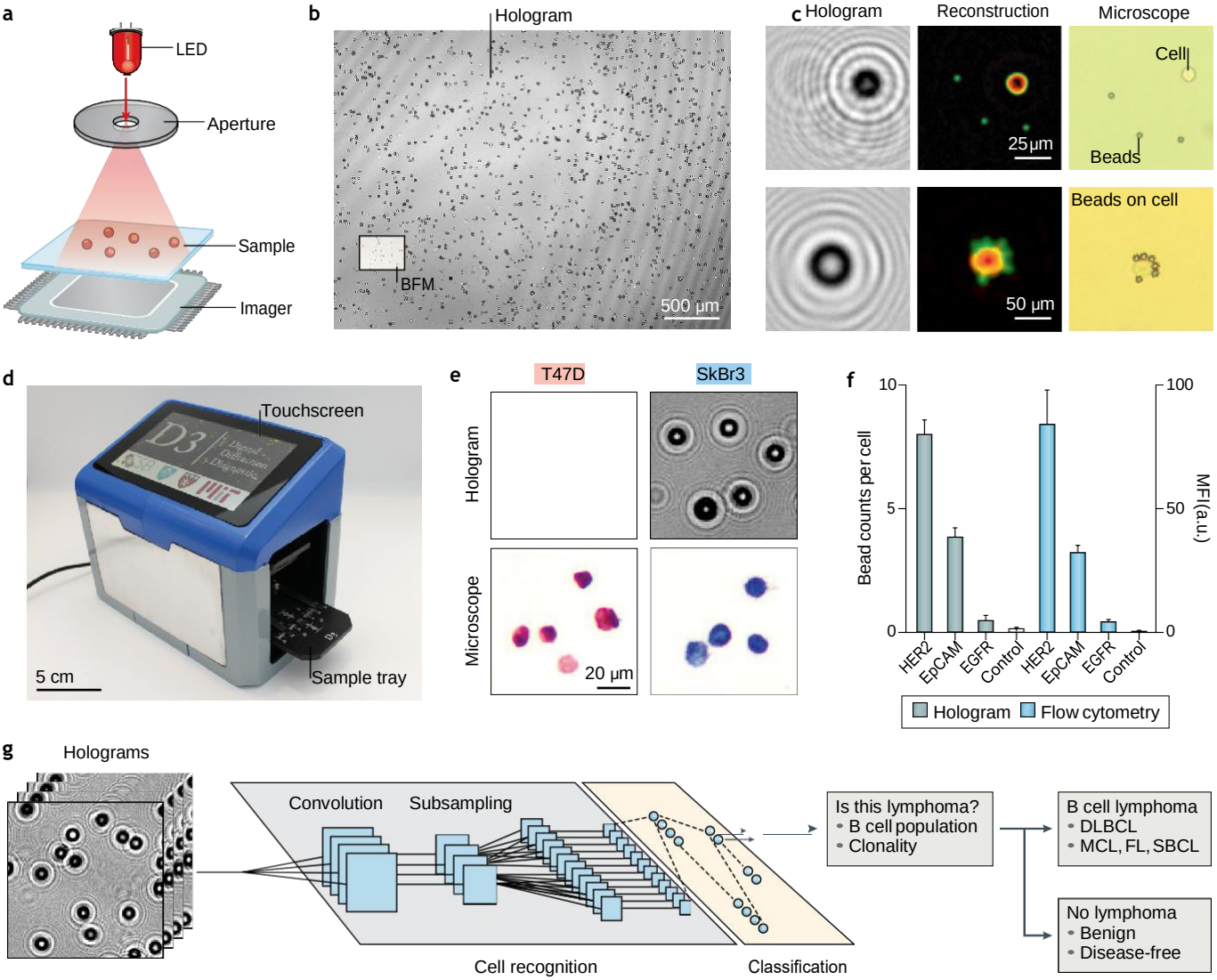

Fig. 3 | **LDIH. a** | Imaging configuration in lens-free digital in-line holography (LDIH). The system consists of a light-emitting diode (LED), an aperture and an imager, with a sample placed directly above the imager. **b** | Wide-field-of-view hologram captured by the LDIH imaging system. The individual block dots are cells, and the black box indicates the field of view of a ×20 bright-field microscope (BFM). **c** | Raw holograms show undecipherable patterns but the numerical image reconstruction recovers object images. The reference BFM images were taken at ×20 magnification. **d** | A portable, stand-alone LDIH device built and used for point-of-care cancer diagnostics. Recorded holograms are transferred to a remote server for image reconstruction. **e** | Human T47D and SkBr3 breast cancer cells were stained for the oestrogen receptor/progesterone receptor (red) and human epidermal growth factor receptor 2 (HER2; blue) and imaged via LDIH and BFM. Note that the hologram contrast changed according to the staining level. **f** | Cells were labelled for different biomarkers and analysed by LDIH and flow cytometry. Note that hologram-based and flow-cytometry-based analysis of biomarker expression is generally concordant. **g** | Deep-learning algorithms for hologram analyses. A convolutional neural network identifies labelled cells directly from holograms. Images classified as cells enter the next module for colour classification. The final information is used for lymphoma diagnostics. DLBCL, diffuse large B cell lymphoma; EGFR, epidermal growth factor receptor; EpCAM, epithelial cell adhesion molecule; FL, follicular lymphoma; MCL, mantle-cell lymphoma; MFI, mean fluorescence intensity; SBCL, spindle B cell lymphoma. Panels **a** and **b** are adapted with permission from REF.[31], American Chemical Society. Panel **c** is adapted with permission from REF.[45], Proceedings of the National Academy of Sciences. Panel **d** is adapted from REF.[32], Springer Nature Limited. Panel **e** is adapted with permission from REF.[31], American Chemical Society. Panel **f** is adapted with permission from REF.[45], Proceedings of the National Academy of Sciences.

reduce system size (2.4 cm^3, 1.9 g)[62]. Such a small form factor allows the scope to be mounted on an animal's head with minimal interruption to its natural behaviour[63,64] for imaging of live fluorescently tagged cells. As potential point-of-care applications, miniscopes have been used for cell profiling and bacterial detection[62] (FIG. 5b). In addition, a miniscope array can perform large-area imaging without scanning, taking advantage of the scope's small lateral size (~5 mm). The miniscope design is now in the public domain as an open-source microscope[65], promoting new ideas and functional extension. System modification and computational processing have enabled two-photon excitation[66], volumetric rendering[67] and lensless imaging[68].

For simultaneous multicolour (≥4) cellular analyses, we recently developed the Cytometry Portable Analyser (CytoPAN) system, which was originally built for operation in remote locations (FIG. 5c) but has since been applied in point-of-care settings (for example, in the operating room, interventional suites and doctors' offices). In this system, the excitation light sources are positioned for side illumination through a glass slide, and a single emission filter with four passbands is used; no dichroic mirrors or mechanical filter changes are necessary. Furthermore, intelligent software can be used to streamline the entire assay, including light-source calibration, sample-slide detection, data acquisition and cellular analyses. CytoPAN has four different fluorescent channels (FIG. 5d) and a bright-field imaging capacity. As proof-of-concept of its utility, automated CytoPAN software algorithms were shown to be capable of analysing individual cells and producing summary reports to inform cancer diagnosis (FIG. 5e). This affordable system (<$3,500), which is operable by non-skilled workers, is currently undergoing field testing in low-income and middle-income countries.

As these fluorescent systems are still bound by the physical SBP limit, a trade-off between FOV and spatial resolution remains. Computational methods used in coherent imaging cannot be applied because fluorescent emission does not carry phase information. New approaches for wide-FOV fluorescent imaging still need further improvement in image quality[68,69]. For now, a straightforward workaround is to combine sample scanning with miniaturized optics; a key technical requirement is to automate such operations, including stage movement and imaging stitching. Equally important is the development of tools for reliable sample preparation, for example, by connecting fluidic cartridges with cost-effective pumping systems[70]. This approach would

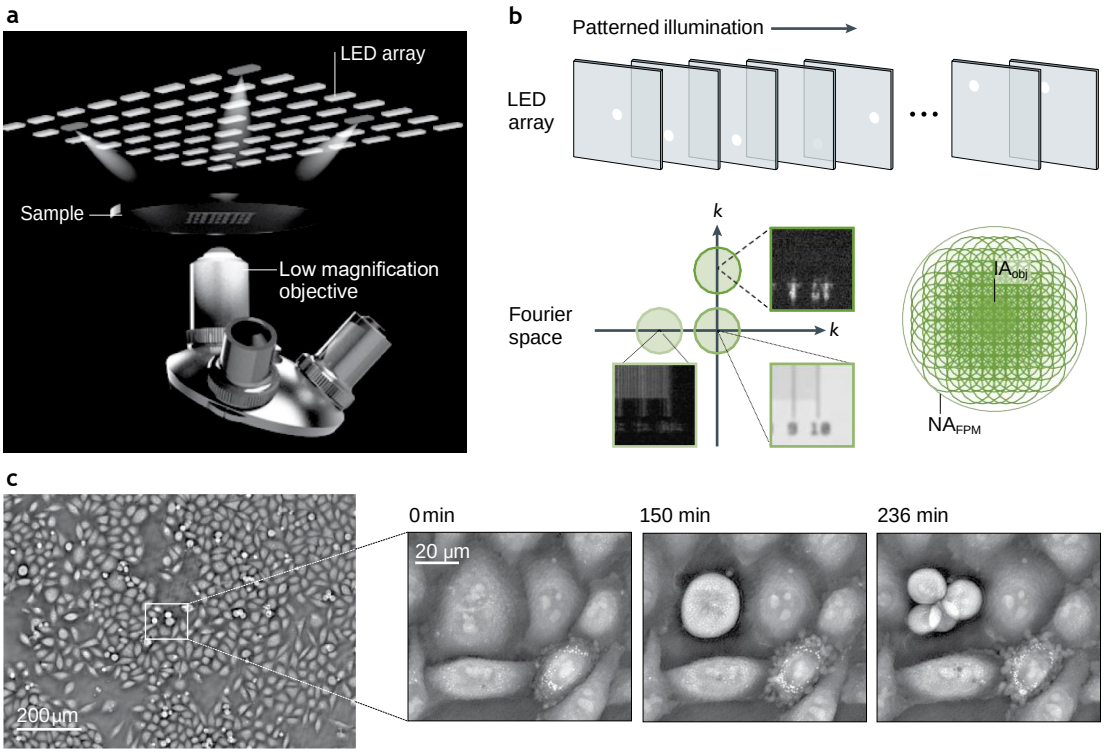

Fig. 4 | **FPM. a** | In a Fourier ptychography microscopy (FPM) system, an array of light-emitting diodes (LEDs) is used for angled illumination and low-magnification-objective lenses capture large-field-of-view (FOV) images. **b** | Sequential images at different illumination patterns are acquired. Each image, bounded by the numerical aperture (NA) of an objective lens (NA_{obj}), contains a patch of frequency information from different regions of the sample's Fourier space. Numerical reconstruction stitches these patches together to cover a larger frequency domain. The effective numerical aperture of the system (NA_{FPM}) is $NA_{obj} + NA_{light}$, where NA_{light} is the numerical aperture of the illumination source. **c** | A full-FOV FPM image reconstruction of human HeLa cells. The image, taken with a ×4 objective lens, achieved a ×0.8 NA resolution and has a FOV of 2.1 × 1.8 mm^2. The time-lapse images (reconstructed from a zoom-in of the original image; white box) reveal a cell undergoing mitosis (that is, dividing into multiple daughter cells), highlighting the ability of FPM to show subcellular detail. Indeed, globular daughter cells, which would have been blurred in conventional high-magnification microscopy, remain in focus with FPM. Panel **c** is adapted with permission from REF.[57], The Optical Society.

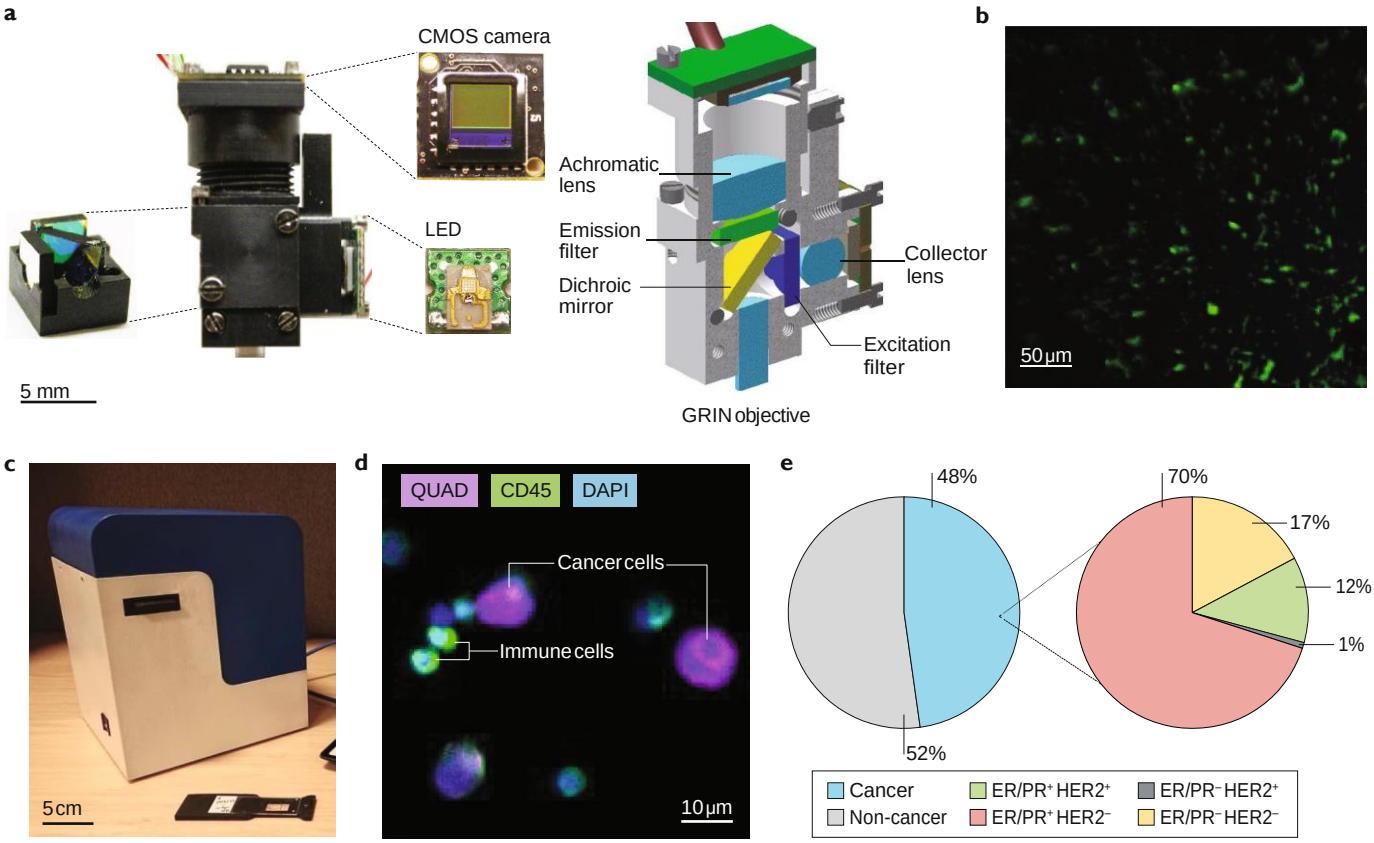

Fig. 5 | **Miniaturized fluorescent cytometers. a** | In thumb-sized fluorescent microscopes ('miniscopes'), a finger-sized, single-channel fluorescent microscope is structured like a conventional fluorescent microscope but uses a light-emitting diode (LED) as an excitation source and a gradient refractive index (GRIN) lens as an objective lens. **b** | The miniscope was used to image *Mycobacterium tuberculosis* stained with the fluorescent dye auramine O. The image shows a 300 × 300-pixel region of the complementary metal–oxide–semiconductor (CMOS) camera. **c** | The Cytometry Portable Analyser (CytoPAN) system is currently under development and integrates five light sources and a quad-band filter. No mechanical parts are necessary for multiple-channel imaging. **d** | Upon CytoPAN-based analysis of a fine-needle aspiration specimen from a patient with breast cancer, cancer cells are identified through the staining of 'quad markers' (QUAD) — epidermal growth factor receptor, epithelial cell adhesion molecule, human epidermal growth factor receptor 2 (HER2) and mucin 1, or epidermal growth factor receptor, epithelial cell adhesion molecule, cytokeratins and mucin 1 — and immune cells are identified through CD45 staining. Images are taken at ×5 magnification. **e** | CytoPAN software automatically profiles individual cells in multicolour channels and generates a summary report to guide cancer diagnosis. From the total cell counts, the proportion of cancer cells (QUAD positive) is obtained (left) and further stratified according to the expression levels of oestrogen receptor (ER)/progesterone receptor (PR) and HER2. Panels **a** and **b** are adapted from REF.[62], Springer Nature Limited. Panels **c**, **d** and **e** courtesy of J. Min and L. K. Chin.

increase the speed of assays and minimize procedural errors, particularly in cyclic imaging, which requires repeated fluidic handling (quenching, washing and labelling).

Machine learning for imaging analyses

Manually inspecting and analysing images produced by the aforementioned systems is time-consuming, impractical, subject to the bias of the operators and requires trained specialists who are often scarce in low-income and middle-income countries. Machine learning has emerged as an indispensable tool to effectively address these challenges. Classic machine-learning tools, such as logistic regression, learn to make inferred decisions based on an input of preselected data features[71]. Such features are typically manually selected and serve to condense complex information (for example, a whole-cell image) into a smaller set of numeric variables (such as size and shape). By contrast, deep-learning tools simultaneously learn to extract relevant features from complex input data and to manipulate those features to perform specified tasks[71]. With exposure to training examples, deep-learning algorithms incrementally update data-transformation parameters to improve task performance. Once fully trained, models can be further improved through continuous exposure to new data sets.

Computational platforms for machine learning and dedicated imaging software. In deep learning, convolutional neural networks (CNNs) are the most widely used architectures for cellular-imaging analyses, due to their strong performance in the analysis of spatial information[72,73] (BOX 1; FIG. 6a). CNNs are designed to process data with array-like structures, such as images, which are 2D arrays of pixels. Machine-learning models can be built with most existing programming languages

Box 1 | **Key concepts in CNNs**

In deep learning, convolutional neural networks (CNNs) are the most widely used architectures for cellular-imaging analyses. The principal concepts employed in CNN development are outlined here.

Convolution

This operation takes an input, multiplies it with a weight matrix (also termed a kernel or filter) and produces summed output layers[121]. The weight matrix is much smaller than the input, and the output layer, or feature map, displays an input's response to a particular filter. Each element of the feature map is based on a small number of neighbouring input elements (sparse interactions), and different regions of the feature map are produced by the same filter parameters (parameter sharing). These two properties dramatically minimize the number of parameters when evaluating the whole input. Convolution effectively finds localized but generalizable structures. Global interaction is still preserved through successive convolution operations; output elements in a deeper convolution layer are indirectly connected to larger numbers of input elements.

Activation functions

In CNNs, information flows unidirectionally through network layers. Activation functions bridge two adjacent networks, transforming the output of a preceding network and feeding it to the following one. Activations are necessary to make the entire network non-linear and to, therefore, increase its capacity for problem-solving. The most common function is a rectified linear unit (ReLU)[122,123] with the form $a(x) = \max(0, x)$. Another popular function is softmax, which takes number outputs from a convolution layer and converts them into the probability distributions for potential outcomes[124].

Pooling

The output from an activation function can go through a pooling operation, which replaces each output element with a summary statistic of its neighbourhood. CNNs often use the max pooling, which reports the maximum value within a rectangular neighbourhood[125]. Pooling downsamples the output by the neighbourhood size, and also makes the network invariant to minute changes in inputs. For example, the pooled output can be the same even if certain features are translated by a few pixels in images.

Training and testing

Building a CNN for a given task usually involves two steps — a new model learns to optimize its parameters using a training data set and the trained model is applied to previously unseen inputs (a test data set) to assess generalization. Underfitting occurs when the training error is above a preset threshold. Overfitting occurs when the training error is much less than the generalization error.

Regularization

Underfitting can be resolved by expanding the model's learning capacity, typically by increasing the number of network parameters. Reducing overfitting, however, requires more systematic strategies that are collectively called regularization. One such technique, dropout, stands out as computationally efficient and broadly applicable[126]. At a predefined probability (dropout rate), dropout intentionally removes the output elements from intermediate networks. This stochastically mimics evaluating an ensemble of models with different subnetwork structures. The final model can, therefore, be more generalizable to a given task.

Data augmentation

The accuracy of a neural network improves as more data are used for training. Data augmentation expands training data sets by creating artificial data[77]. The method has been particularly effective for image-classification problems. Cell images, for example, can be pixel-shifted, rotated or mirrored without losing a real-world context.

Hyperparameters

As settings that define a model architecture and control learning processes, hyperparameters exist outside of the model's domain and must be set externally. Search algorithms such as grid search and Bayesian optimization can be used to automate hyperparameter optimization by forming a wrapper around a learning model. This approach, however, is computationally expensive. In most cases, tuning hyperparameters is a heuristic process, largely relying on programmers' experience.

Transfer learning

A model trained for one task can be reused to solve a second related task if the tasks share common features[127]. For example, a CNN optimized for cancer-cell detection can be retrained to identify other cell types. In this case, the transferred network serves as an initial instance to be fine-tuned for a new task. In another form, an unaltered, pretrained network is concatenated with additional networks, wherein the pretrained network is used to capture general features. Transfer learning can narrow the scope of possible models to be searched[51].

(C, C++, Java, MATLAB, Python or R), and new languages, such as Julia, have been developed for faster computation. The de facto language for machine learning, however, is Python, the popularity of which has been boosted among data scientists by the release of TensorFlow, a computational framework for machine learning, in the Python application programming interface[74]. Various machine-learning frameworks are also available (for examples, see Supplementary Table 1), providing convenient building blocks as well as GPU-compatible libraries for accelerated computation.

The organization of computational layers, referred to as the model architecture, depends on the analysis task. Although frameworks exist for designing novel architectures, researchers might opt for predefined models with established success. For image-to-image transformations, such as single-cell segmentation, the U-Net[75] and DeepLab[76] architectures are two popular choices. These models encode images into information-rich features by convolution and then deconvolve them to produce segmentation images at input resolution. By contrast, classification tasks use feature encodings to produce a probability distribution among classes. These CNN architectures typically differ in the building blocks that make up the encoding process. Popular architectures include AlexNet[77], ResNet[78], VGG[79] and Inception[80].

Stand-alone imaging software now tends to integrate learning capacities in its design[81–86] (Supplementary Table 2). These tools make it possible to build machine-learning models in a coding-free, user-friendly environment, but analysis might be limited to predefined tasks. Some software expands its flexibility by incorporating support for script interpretation or communication with external programs.

Machine learning in conventional cytopathology. Conventional cytopathology incorporates computational approaches in the form of automated slide analysis and whole-slide imaging. These approaches still rely on expert and optimized slide preparation, state-of-the art microscopes and slide scanners (which often cost more than $100,000) and specialists to analyse flagged abnormalities. Nevertheless, these approaches and their clinical use provide important lessons from which the

next generation of automated image-cytometry systems can benefit[14].

There are currently three commercial systems that use proprietary algorithms to analyse Pap-stained cervical-cytology slides — the ThinPrep Imaging System (Hologic, Marlborough, MA), the FocalPoint GS Imaging System (Becton Dickinson, Franklin Lakes, NJ) and BestCyte (CellSolutions, Greensboro, NC)[17,87]. Beyond these systems, experimental studies have used machine learning to automate nuclear morphometry for the analysis of breast-cancer[15,16,88,89] cells and other malignancies[17].

Cellular analyses based on machine learning. In addition to facilitating conventional tasks in image analyses[75,90–95], the power of machine learning to discover and generalize hidden patterns could advance new paradigms in cytometry.

For example, in the case of in silico labelling, a deep neural network learned to predict fluorescent labels from unstained bright-field micrographs[96] (FIG. 6b). The network was trained on paired images of unlabelled and fluorescently labelled cells. The use of *z*-stacks of bright-field images improved prediction accuracy,

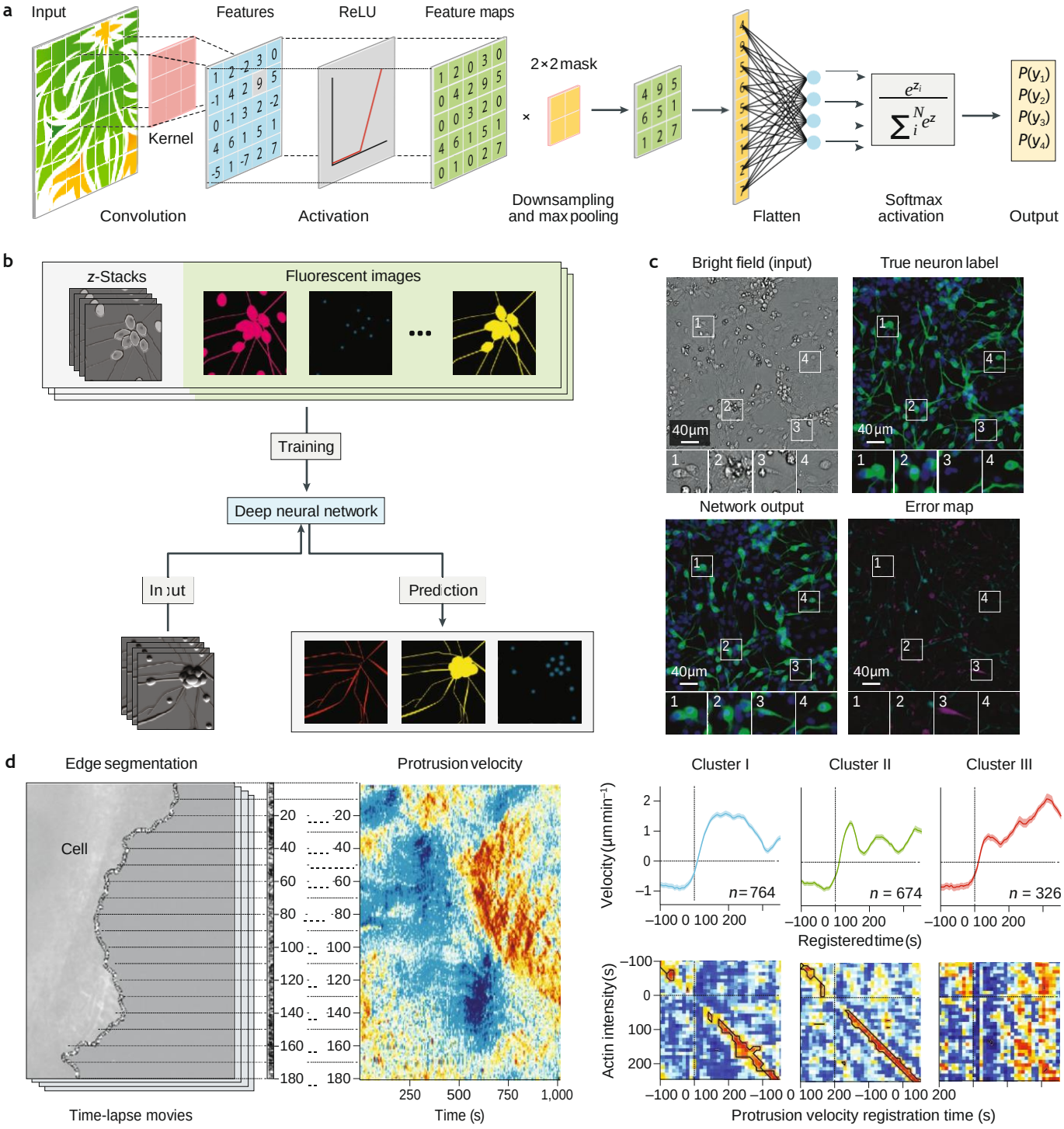

presumably by increasing the morphological information available for feature extraction. Indeed, the network reported smaller errors as more distinct *z*-stack images were used. By predicting cellular labelling, the trained model could identify cell types and cell state (FIG. 6c). Furthermore, the knowledge was transferrable; once trained to predict a set of labels, the network could learn new labels from a small number of additional data sets, effectively demonstrating transfer learning (BOX 1).

Machine learning has also effectively determined heterogeneous cellular phenotypes that otherwise would be obscured in complexity. For example, a computational approach was developed to analyse subcellular protrusion activities in time-lapse micrographs[97] (FIG. 6d). Without supervision, the framework resolved different protrusion velocities and mapped them into three distinct clusters, revealing a previously unknown 'accelerating protrusion'. Interestingly, the protrusion phenotypes could be associated with actin regulator dynamics, highlighting how machine learning might help to discover unknown molecular mechanisms.

Clinical cytometry applications

The technical requirements for diagnosis vary among different cancer types. Below are some practical examples highlighting the use of new cytometry methods.

Lymphoma. One of the major health challenges in sub-Saharan Africa is the high prevalence of AIDS-related cancers (sometimes termed the 'second wave of AIDS')[98–100]. Some such cancers, for example, diffuse large B cell lymphoma (DLBCL) and Burkitt lymphoma, are very aggressive. However, owing to limited resources, many patients with these malignancies evade comprehensive evaluation or are not appropriately classified. Diagnosis and care are often hampered by an inability to acquire proper tissue specimen, lack of diagnostic reagents, limited availability of specialists and low access to care in rural settings. Although a major portion of these cases are curable (even in low-income and middle-income countries), therapeutic opportunities are often missed[101,102].

In 2018, a prospective clinical trial used the contrast-enhanced LDIH system and the aforementioned deep-learning algorithm on percutaneously obtained FNA samples from 40 patients who were clinically referred for aspiration and biopsy of enlarged lymph nodes (lymphadenopathy) detected by whole-body imaging that were suspicious of lymphoma[32]. Freshly harvested FNA samples were captured on glass slides via CD19/CD20 antibodies and incubated with antibody-coated beads (targeting immunoglobulin κ or λ light chains or Ki67) of unique sizes, absorbancies and holographic signatures. Bead binding to cells was holographically measured and the end result was a quantitative read-out of malignant cell numbers and differentiation between high-grade and low-grade lymphoma subtypes. The automated method was surprisingly accurate and fast, with 91% sensitivity, 100% specificity and 95% accuracy for diagnosing lymphoma and 86% accuracy in triaging lymphomas into aggressive and indolent types. No false positives were found for benign or disease-free samples, and only one sample was non-diagnostic due to low B cell counts. By comparison, clinical flow cytometry showed 10 non-diagnostic cases with 87% accuracy for diagnosing lymphoma. More importantly, flow cytometry either could not or failed to distinguish aggressive from indolent types. Larger-scale trials are currently underway in HIV-endemic regions of Africa.

Breast cancer. Breast-cancer diagnosis and the differentiation between palpable mass lesions and benign lesions is another considerable problem in low-income and middle-income countries with severe diagnostic bottlenecks. Artificial Intelligence Diffraction Analysis (AIDA), a low-cost digital system based on computational optics and deep learning, was designed to diagnose breast cancer from FNA samples[31]. Unlike the bead-based microholography in lymphoma[32], AIDA uses chromogenic stains with enzyme-mediated amplification to resolve receptor status in harvested cells. A promising early study showed high accuracy (>90%) in recognizing cells directly from diffraction patterns and in classifying breast-cancer types using deep-learning-based analysis of sample aspirates. The image algorithm was fast, enabling cellular analyses at high throughput (~3 s per 1,000 cells), and the automated workflow enables use by less skilled healthcare workers. For global healthcare applications, the system is currently being adapted for even simpler operation[31]. Additionally, large-scale trials of the fluorescence multiplexing technology (CytoPAN) are underway.

Oral cancer. Over 90% of oral cancers are squamous-cell carcinomas. These head and neck squamous-cell carcinomas are the sixth leading cancer by incidence worldwide, with more than 550,000 cases and ~300,000 deaths per year, and are very common in parts of the world that

Fig. 6 | **Machine learning in imaging analyses. a** | Key concepts in convolutional neural networks are shown. Convolution followed by activation extracts features, and the pooling operation downsamples intermediate layers while keeping salient features. 2D feature maps are then reshaped into a vector (flattening) and, following traditional neural network layers, a softmax activation produces a final probability distribution for classification. **b** | In the case of in silico labelling, machine learning has been used to predict fluorescent labelling from unlabelled images and to infer cell type. By using *z*-stacks of transmitted and fluorescent micrographs as training sets, a convolution neural network learned to predict fluorescent labelling from unlabelled images. **c** | The in silico labelling approach was applied to predict cell type. The input image (bright field) contains various cell types differentiated from pluripotent stem cells. In the ground-truth image, cells were stained for neuron-specific class III β-tubulin (TuJ1; green) and nucleus (Hoechst; blue). The network was trained to predict the intensity of these labels at each pixel. In the error map, predicted pixels that are too bright (false positives) are displayed in magenta and those that are too dim (false negatives) are displayed in teal. Outsets 1, 2 and 4 show correct predictions but note that outset 3 shows a false positive — a cell that has neuronal morphology but is not TuJ1 positive. **d** | Machine learning has also shown promise for subcellular-feature analysis. A leading edge of a migrating cell was imaged over time. The cell boundary was segmented into small probing windows and the protrusion velocity in each window was tracked. Unsupervised machine learning grouped protrusion activities into three clusters. Cluster III is a previously unknown phenotype, 'accelerating protrusion', whereas clusters I and II showed a high correlation between protrusion velocities and actin activities. The results imply that actin nucleation might mediate subcellular protrusion. Cluster III had no distinct pattern, suggesting different actin molecular dynamics. ReLU, rectified linear unit. Panels **b** and **c** are adapted with permission from REF.[96], Elsevier. Panel **d** is adapted from REF.[97], CC-BY-4.0 (https://creativecommons.org/licenses/by/4.0/).

have high rates of tobacco use, betel use and/or human papillomavirus infection[103,104]. As not all oral lesions are malignant, biopsy-based histopathological diagnosis is essential. In prior research, a fluorescently labelled poly(ADP-ribose) polymerase (PARP) inhibitor (PARPi-FL) was developed as an intravital fluorescent dye to be used in point-of-care settings[105–108]. Studies from the past 5 years have shown the feasibility of using PARPi-FL as a quantitative biomarker for oral cancer[106]. Preliminary results from a first-in-human trial (NCT03085147)[108] devised a PARPi-FL topical-staining protocol for human biospecimens. Using fresh oral-cancer tissues within 25 min of biopsy, the protocol correctly identified cancer and margin samples with >95% sensitivity and specificity. The study also showed that PARPi-FL imaging can be integrated into clinical workflows to instantaneously assess the presence or absence of microscopic disease at the surgical margin.

Diagnosing cancer in fluid samples. Numerous bodily fluids can be readily sampled with small needles and subsequently analysed for cancer cells. Such procedures include paracentesis, thoracentesis and cyst-fluid aspiration, all of which are often performed either therapeutically to relieve symptoms or for diagnosis. Conventionally processing such samples still requires labour-intensive concentration, embedding, staining and review. In 2013, a microfluidic-chip platform was developed to enrich cancer cells from highly heterogeneous peritoneal fluid and then perform molecular analyses. Using four of the most promising biomarkers (EpCAM, calretinin, CD45 and vimentin) and 47 patients, the results showed that the marker set can sensitively and specifically map cancer cell numbers and, through its reliable enrichment, facilitate additional treatment-response measurements related to proliferation, protein translation or pathway inhibition[34].

Future perspective

We have reviewed the technical features of new imaging cytometers and their potential for integrated analysis of scant cancer samples. Below, we discuss key milestones to advance the clinical translation and adoption of these new technologies.

Implementation and dissemination. In contemporary laboratory medicine, virtually all blood and urine tests have been automated to reduce cost, improve test quality and accommodate the increasing volume of clinical samples[18,19] (TABLE 1). We argue that this automation should also be possible for FNA-based analysis of cancer samples, particularly in resource-limited environments. Furthermore, an expected rise in minimally invasive procedures combined with a shortage of trained cytopathologists will likely exacerbate the need for automated hardware and software solutions in such settings. Moving forward, a key consideration is what will be required to make the development of new technology a clinical reality.

We are still in the research phase of developing and testing integrated solutions. Once accomplished, the merging of technologies and approaches will need to be rigorously tested in prospective clinical trials and different settings. Preferably, these efforts must continue at a large scale and in varied environments. The latter is particularly important, as AI approaches have been shown to be location dependent[109]. In the end, adopting any new technology will require concerted efforts and investment from all parties involved. We direct interested readers to other reviews that have extensively covered the road map towards the ultimate clinical translation of diagnostic platforms[110,111].

New materials and integrated optics. Paradigms in optical system design are changing — conventional discrete free-space optics, the mainstay since the invention of microscopes, is moving towards integrated precision optoelectronics. Novel material engineering and fabrication technologies drive such transitions. Planar optical waveguides[112], adaptive microlenses[113] and meta materials[114,115] have demonstrated potential for effective beam steering and shaping, and tiny semiconductor chips are readily available for light generation and detection. Multi-material manufacturing can assemble these parts into hybrid devices. For instance, optical components (lenses, filters and waveguides) can be defined in transparent polymer layers[116] and be coupled to semiconductor modules. Hybrid optical sensors are already in production for oximetry and heart-rate monitoring (MAX30102, Maxim). The next step is to expand into optical imaging to create on-chip microscopy technologies.

Future capabilities. One of the most exciting opportunities in this field is new technological capabilities that could be implemented for automated point-of-care cytometry, including the rigorous evaluation of cellular markers and staining techniques and kits. As optoelectronics become even more affordable and integrated, they might incorporate charge-coupled devices with larger FOVs and similar or smaller pixel sizes. Together with larger FOV lenses, this will improve the spatial resolution of images and, ultimately, enable subcellular-image analysis. Computational power and advanced machine-learning algorithms should accelerate reconstructions and improve automated analysis.

Automated, AI-based diagnostic DNA karyometry is another application of interest. A number of studies have tested this method[117–120], but mostly in flow cytometers or manually, rather than by automated image cytometry. An additional unexplored frontier is the molecular testing of cytology samples. Fluorescence in situ hybridization (FISH) using probes with specificity for mutations in the *EGFR*, *KRAS* and *BRAF* genes and other cytogenetic abnormalities should be feasible with appropriate amplification strategies[117]. Finally, the techniques for analysing FNA specimens for cancer diagnosis and monitoring will likely apply almost equally well to other specimen types and diagnostic applications. Inexpensive automated cellular analyses and molecular testing could be contemplated for organ FNA obtained from liver, kidney or blood and/or bone marrow.

Published online: 05 March 2020

1. Weissleder, R., Schwaiger, M. C., Gambhir, S. S. & Hricak, H. Imaging approaches to optimize molecular therapies. *Sci. Transl Med.* **8**, 355ps16 (2016).
2. Frenk, N. E. et al. High-content biopsies facilitate molecular analyses and do not increase complication rates in patients with advanced solid tumors. *JCO Precis. Oncol.* **1**, 1–9 (2017).
3. Capitanio, A., Dina, R. E. & Treanor, D. Digital cytology: A short review of technical and methodological approaches and applications. *Cytopathology* **29**, 317–325 (2018).
4. Asthana, V. et al. An inexpensive, customizable microscopy system for the automated quantification and characterization of multiple adherent cell types. *PeerJ* **6**, e4937 (2018).
5. Balsam, J., Bruck, H. A. & Rasooly, A. Mobile flow cytometer for mHealth. *Methods Mol. Biol.* **1256**, 139–153 (2015).
6. Molnár, B. et al. Circulating cell-free nucleic acids as biomarkers in colorectal cancer screening and diagnosis — an update. *Expert Rev. Mol. Diagn.* **19**, 477–498 (2019).
7. Shao, H. et al. New technologies for analysis of extracellular vesicles. *Chem. Rev.* **118**, 1917–1950 (2018).
8. Sandlin, R. D. et al. Ultra-fast vitrification of patient-derived circulating tumor cell lines. *PLOS ONE* **13**, e0192734 (2018).
9. Sarioglu, A. F. et al. A microfluidic device for label-free, physical capture of circulating tumor cell clusters. *Nat. Methods* **12**, 685–691 (2015).
10. Cristofanilli, M. et al. The clinical use of circulating tumor cells (CTCs) enumeration for staging of metastatic breast cancer (MBC): International expert consensus paper. *Crit. Rev. Oncol. Hematol.* **134**, 39–45 (2019).
11. No authors listed. First comprehensive companion diagnostic OK'd. *Cancer Discov.* **8**, OF4 (2018).
12. Van Hoeck, A., Tjoonk, N. H., van Boxtel, R. & Cuppen, E. Portrait of a cancer: mutational signature analyses for cancer diagnostics. *BMC Cancer* **19**, 457 (2019).
13. Hannouf, M. B. et al. Cost-effectiveness analysis of multigene expression profiling assays to guide adjuvant therapy decisions in women with invasive early-stage breast cancer. *Pharmacogenomics J.* **20**, 27–46 (2020).
14. Saha, M., Mukherjee, R. & Chakraborty, C. Computer-aided diagnosis of breast cancer using cytological images: a systematic review. *Tissue Cell* **48**, 461–474 (2016).
15. Filipczuk, P., Fevens, T., Krzyzak, A. & Monczak, R. Computer-aided breast cancer diagnosis based on the analysis of cytological images of fine needle biopsies. *IEEE Trans. Med. Imaging* **32**, 2169–2178 (2013).
16. Dey, P., Logasundaram, R. & Joshi, K. Artificial neural network in diagnosis of lobular carcinoma of breast in fine-needle aspiration cytology. *Diagn. Cytopathol.* **41**, 102–106 (2013).
17. Landau, M. A. & Pantanowitz, L. Artificial intelligence in cytopathology: a review of the literature and overview of commercial landscape. *J. Am. Soc. Cytopathol.* **8**, 230–241 (2019).
18. Stephens, L., Bevins, N. J., Bengtsson, H. I. & Broome, H. E. Comparison of different small clinical hematology laboratory configurations with focus on remote smear imaging. *Arch. Pathol. Lab. Med.* **143**, 1234–1245 (2019).
19. Andrade, A. R. et al. Recent computational methods for white blood cell nuclei segmentation: a comparative study. *Comput. Methods Prog. Biomed.* **173**, 1–14 (2019).
20. Prieto, S. P., Powless, A. J., Boice, J. W., Sharma, S. G. & Muldoon, T. J. Proflavine hemisulfate as a fluorescent contrast agent for point-of-care cytology. *PLOS ONE* **10**, e0125598 (2015).
21. Lin, J. R., Fallahi-Sichani, M. & Sorger, P. K. Highly multiplexed imaging of single cells using a high-throughput cyclic immunofluorescence method. *Nat. Commun.* **6**, 8390 (2015).
22. Gerdes, M. J. et al. Highly multiplexed single-cell analysis of formalin-fixed, paraffin-embedded cancer tissue. *Proc. Natl Acad. Sci. USA* **110**, 11982–11987 (2013).
23. Schubert, W. et al. Analyzing proteome topology and function by automated multidimensional fluorescence microscopy. *Nat. Biotechnol.* **24**, 1270–1278 (2006).
24. Giedt, R. J. et al. Single-cell barcode analysis provides a rapid readout of cellular signaling pathways in clinical specimens. *Nat. Commun.* **9**, 4550 (2018).
25. Ullal, A. V. et al. Cancer cell profiling by barcoding allows multiplexed protein analysis in fine-needle aspirates. *Sci. Transl Med.* **6**, 219ra9 (2014).
26. Agasti, S. S., Liong, M., Peterson, V. M., Lee, H. & Weissleder, R. Photocleavable DNA barcode–antibody conjugates allow sensitive and multiplexed protein analysis in single cells. *J. Am. Chem. Soc.* **134**, 18499–18502 (2012).
27. Kishi, J. Y. et al. SABER amplifies FISH: enhanced multiplexed imaging of RNA and DNA in cells and tissues. *Nat. Methods* **16**, 533–544 (2019).
28. De Wit, S. et al. Classification of cells in CTC-enriched samples by advanced image analysis. *Cancers* **10**, 377 (2018).
29. Haun, J. B. et al. Micro-NMR for rapid molecular analysis of human tumor samples. *Sci. Transl Med.* **3**, 71ra16 (2011).
30. Yang, K. S. et al. Multiparametric plasma EV profiling facilitates diagnosis of pancreatic malignancy. *Sci. Transl Med.* **9**, eaal3226 (2017).
31. Min, J. et al. Computational optics enables breast cancer profiling in point-of-care settings. *ACS Nano* **12**, 9081–9090 (2018).
32. Im, H. et al. Design and clinical validation of a point-of-care device for the diagnosis of lymphoma via contrast-enhanced microholography and machine learning. *Nat. Biomed. Eng.* **2**, 666–674 (2018).
33. Ghazani, A. A. et al. Molecular characterization of scant lung tumor cells using iron-oxide nanoparticles and micro-nuclear magnetic resonance. *Nanomedicine* **10**, 661–668 (2014).
34. Peterson, V. M. et al. Ascites analysis by a microfluidic chip allows tumor-cell profiling. *Proc. Natl Acad. Sci. USA* **110**, E4978–E4986 (2013).
35. Marquard, A. N., Carlson, J. C. T. & Weissleder, R. Glass chemistry to analyze human cells under adverse conditions. *ACS Omega* **4**, 11515–11521 (2019).
36. Lohmann, A. W., Dorsch, R. G., Mendlovic, D., Ferreira, C. & Zalevsky, Z. Space–bandwidth product of optical signals and systems. *J. Opt. Soc. Am. A* **13**, 470–473 (1996).
37. Van Es, S. L. et al. Constant quest for quality: digital cytopathology. *J. Pathol. Inform.* **9**, 13 (2018).
38. Hu, B., Bolus, D. & Brown, J. Q. Improved contrast in inverted selective plane illumination microscopy of thick tissues using confocal detection and structured illumination. *Biomed. Opt. Express* **8**, 5546–5559 (2017).
39. Wang, M. et al. Gigapixel surface imaging of radical prostatectomy specimens for comprehensive detection of cancer-positive surgical margins using structured illumination microscopy. *Sci. Rep.* **6**, 27419 (2016).
40. Garcia-Sucerquia, J. et al. Digital in-line holographic microscopy. *Appl. Opt.* **45**, 836–850 (2006).
41. Gurkan, U. A. et al. Miniaturized lensless imaging systems for cell and microorganism visualization in point-of-care testing. *Biotechnol. J.* **6**, 138–149 (2011).
42. Zheng, G., Lee, S. A., Antebi, Y., Elowitz, M. B. & Yang, C. The ePetri dish, an on-chip cell imaging platform based on subpixel perspective sweeping microscopy (SPSM). *Proc. Natl Acad. Sci. USA* **108**, 16889–16894 (2011).
43. Kim, S. B. et al. A cell-based biosensor for real-time detection of cardiotoxicity using lensfree imaging. *Lab. Chip* **11**, 1801–1807 (2011).
44. Greenbaum, A. et al. Imaging without lenses: achievements and remaining challenges of wide-field on-chip microscopy. *Nat. Methods* **9**, 889–895 (2012).
45. Im, H. et al. Digital diffraction analysis enables low-cost molecular diagnostics on a smartphone. *Proc. Natl Acad. Sci. USA* **112**, 5613–5618 (2015).
46. Rostykus, M., Soulez, F., Unser, M. & Moser, C. Compact in-line lensfree digital holographic microscope. *Methods* **136**, 17–23 (2018).
47. Rappaz, B. et al. Comparative study of human erythrocytes by digital holographic microscopy, confocal microscopy, and impedance volume analyzer. *Cytometry A* **73**, 895–903 (2008).
48. Seo, S. et al. High-throughput lens-free blood analysis on a chip. *Anal. Chem.* **82**, 4621–4627 (2010).
49. Mudanyali, O., Bishara, W. & Ozcan, A. Lensfree super-resolution holographic microscopy using wetting films on a chip. *Opt. Express* **19**, 17378–17389 (2011).
50. Lee, S. A. et al. Color capable sub-pixel resolving optofluidic microscope and its application to blood cell imaging for malaria diagnosis. *PLOS ONE* **6**, e26127 (2011).
51. Kim, S. J. et al. Deep transfer learning-based hologram classification for molecular diagnostics. *Sci. Rep.* **8**, 17003 (2018).
52. Rivenson, Y., Zhang, Y., Günaydın, H., Teng, D. & Ozcan, A. Phase recovery and holographic image reconstruction using deep learning in neural networks. *Light Sci. Appl.* **7**, 17141 (2018).
53. Greenbaum, A. & Ozcan, A. Maskless imaging of dense samples using pixel super-resolution based multi-height lensfree on-chip microscopy. *Opt. Express* **20**, 3129–3143 (2012).
54. Luo, W., Zhang, Y., Feizi, A., Göröcs, Z. & Ozcan, A. Pixel super-resolution using wavelength scanning. *Light Sci. Appl.* **5**, e16060 (2016).
55. Bao, P., Situ, G., Pedrini, G. & Osten, W. Lensless phase microscopy using phase retrieval with multiple illumination wavelengths. *Appl. Opt.* **51**, 5486–5494 (2012).
56. Ou, X., Horstmeyer, R., Zheng, G. & Yang, C. High numerical aperture Fourier ptychography: principle, implementation and characterization. *Opt. Express* **23**, 3472–3491 (2015).
57. Tian, L. et al. Computational illumination for high-speed in vitro Fourier ptychographic microscopy. *Optica* **2**, 904–911 (2015).
58. Nguyen, T., Xue, Y., Li, Y., Tian, L. & Nehmetallah, G. Deep learning approach for Fourier ptychography microscopy. *Opt. Express* **26**, 26470–26484 (2018).
59. Zheng, G., Horstmeyer, R. & Yang, C. Wide-field, high-resolution Fourier ptychographic microscopy. *Nat. Photonics* **7**, 739–745 (2013).
60. Horstmeyer, R., Chung, J., Ou, X., Zheng, G. & Yang, C. Diffraction tomography with Fourier ptychography. *Optica* **3**, 827–835 (2016).
61. Dong, S. et al. Aperture-scanning Fourier ptychography for 3D refocusing and super-resolution macroscopic imaging. *Opt. Express* **22**, 13586–13599 (2014).
62. Ghosh, K. K. et al. Miniaturized integration of a fluorescence microscope. *Nat. Methods* **8**, 871–878 (2011).
63. Liberti, W. A., Perkins, L. N., Leman, D. P. & Gardner, T. J. An open source, wireless capable miniature microscope system. *J. Neural Eng.* **14**, 045001 (2017).
64. Jacob, A. D. et al. A compact head-mounted endoscope for in vivo calcium imaging in freely behaving mice. *Curr. Protoc. Neurosci.* **84**, e51 (2018).
65. Aharoni, D. & Hoogland, T. M. Circuit investigations with open-source miniaturized microscopes: past, present and future. *Front. Cell. Neurosci.* **13**, 141 (2019).
66. Helmchen, F., Fee, M. S., Tank, D. W. & Denk, W. A miniature head-mounted two-photon microscope. High-resolution brain imaging in freely moving animals. *Neuron* **31**, 903–912 (2001).
67. Skocek, O. et al. High-speed volumetric imaging of neuronal activity in freely moving rodents. *Nat. Methods* **15**, 429–432 (2018).
68. Adams, J. K. et al. Single-frame 3D fluorescence microscopy with ultraminiature lensless FlatScope. *Sci. Adv.* **3**, e1701548 (2017).
69. Ah Lee, S., Ou, X., Lee, J. E. & Yang, C. Chip-scale fluorescence microscope based on a silo-filter complementary metal-oxide semiconductor image sensor. *Opt. Lett.* **38**, 1817–1819 (2013).
70. Almada, P. et al. Automating multimodal microscopy with NanoJ-Fluidics. *Nat. Commun.* **10**, 1223 (2019).
71. LeCun, Y., Bengio, Y. & Hinton, G. Deep learning. *Nature* **521**, 436–444 (2015).
72. LeCun, Y., Bottou, L., Bengio, Y. & Haffner, P. Gradient-based learning applied to document recognition. *Proc. IEEE* **86**, 2278–2324 (1998).
73. Cao, C. et al. Deep learning and its applications in biomedicine. *Genom. Proteom. Bioinform.* **16**, 17–32 (2018).
74. Abadi, M. et al. TensorFlow: a system for large-scale machine learning. Preprint at *arXiv* https://arxiv.org/abs/1605.08695 (2016).
75. Ronneberger, O., Fischer, P. & Brox, T. U-Net: convolutional networks for biomedical image segmentation. *Med. Image Comput. Comput. Assist. Interv.* **9351**, 234–241 (2015).
76. Chen, L.-C., Papandreou, G., Kokkinos, I., Murphy, K. & Yuille, A. L. DeepLab: semantic image segmentation with deep convolutional nets, atrous convolution, and fully connected CRFs. *IEEE Trans. Pattern Anal. Mach. Intell.* **40**, 834–848 (2018).
77. Krizhevsky, A., Sutskever, I. & Hinton, G. E. ImageNet classification with deep convolutional neural networks. *Adv. Neural Inf. Process. Syst.* **1**, 1097–1105 (2012).
78. He, K., Zhang, X., Ren, S. & Sun, J. in *Proc. IEEE Comput. Soc. Conf. Comput. Vis. Pattern Recognit.* 770–778 (IEEE, 2016).
79. Simonyan, K. & Zisserman, A. Very deep convolutional networks for large-scale image recognition. Preprint at *arXiv* https://arxiv.org/abs/1409.1556 (2014).

80. Szegedy, C. et al. in *Proc. IEEE Comput. Soc. Conf. Comput. Vis. Pattern Recognit.* 1–9 (IEEE, 2015).
81. Schindelin, J. et al. Fiji: an open-source platform for biological-image analysis. *Nat. Methods* **9**, 676–682 (2012).
82. Kamentsky, L. et al. Improved structure, function and compatibility for CellProfiler: modular high-throughput image analysis software. *Bioinformatics* **27**, 1179–1180 (2011).
83. Held, M. et al. CellCognition: time-resolved phenotype annotation in high-throughput live cell imaging. *Nat. Methods* **7**, 747–754 (2010).
84. Murphy, R. F. CellOrganizer: image-derived models of subcellular organization and protein distribution. *Methods Cell Biol.* **110**, 179–193 (2012).
85. Sommer, C., Straehle, C., Koethe, U. & Hamprecht, F. A. in *Proc. IEEE Int. Symp. Biomed. Imaging* 230–233 (IEEE, 2011).
86. Kvilekval, K., Fedorov, D., Obara, B., Singh, A. & Manjunath, B. S. Bisque: a platform for bioimage analysis and management. *Bioinformatics* **26**, 544–552 (2010).
87. Thrall, M. J. Automated screening of Papanicolaou tests: a review of the literature. *Diagn. Cytopathol.* **47**, 20–27 (2019).
88. Kashyap, A., Jain, M., Shukla, S. & Andley, M. Study of nuclear morphometry on cytology specimens of benign and malignant breast lesions: a study of 122 cases. *J. Cytol.* **34**, 10–15 (2017).
89. Subbaiah, R. M., Dey, P. & Nijhawan, R. Artificial neural network in breast lesions from fine-needle aspiration cytology smear. *Diagn. Cytopathol.* **42**, 218–224 (2014).
90. Ouyang, W., Aristov, A., Lelek, M., Hao, X. & Zimmer, C. Deep learning massively accelerates super-resolution localization microscopy. *Nat. Biotechnol.* **36**, 460–468 (2018).
91. Buggenthin, F. et al. Prospective identification of hematopoietic lineage choice by deep learning. *Nat. Methods* **14**, 403–406 (2017).
92. Esteva, A. et al. Dermatologist-level classification of skin cancer with deep neural networks. *Nature* **542**, 115–118 (2017).
93. Gulshan, V. et al. Development and validation of a deep learning algorithm for detection of diabetic retinopathy in retinal fundus photographs. *JAMA* **316**, 2402–2410 (2016).
94. Van Valen, D. A. et al. Deep learning automates the quantitative analysis of individual cells in live-cell imaging experiments. *PLOS Comput. Biol.* **12**, e1005177 (2016).
95. Heo, Y. J., Lee, D., Kang, J., Lee, K. & Chung, W. K. Real-time image processing for microscopy-based label-free imaging flow cytometry in a microfluidic chip. *Sci. Rep.* **7**, 11651 (2017).
96. Christiansen, E. M. et al. In silico labeling: predicting fluorescent labels in unlabeled images. *Cell* **173**, 792–803.e19 (2018).
97. Wang, C. et al. Deconvolution of subcellular protrusion heterogeneity and the underlying actin regulator dynamics from live cell imaging. *Nat. Commun.* **9**, 1688 (2018).
98. Varmus, H. & Kumar, H. S. Addressing the growing international challenge of cancer: a multinational perspective. *Sci. Transl Med.* **5**, 175cm2 (2013).
99. Livingston, J. Cancer in the shadow of the AIDS epidemic in southern Africa. *Oncologist* **18**, 783–786 (2013).
100. Chabner, B. A. et al. Cancer in Botswana: the second wave of AIDS in Sub-Saharan Africa. *Oncologist* **18**, 777–778 (2013).
101. Naresh, K. N. et al. Lymphomas in sub-Saharan Africa – what can we learn and how can we help in improving diagnosis, managing patients and fostering translational research. *Br. J. Haematol.* **154**, 696–703 (2011).
102. Mwamba, P. M. et al. AIDS-related non-Hodgkin's lymphoma in sub-Saharan Africa: current status and realities of therapeutic approach. *Lymphoma* https://doi.org/10.1155/2012/904367 (2012).
103. Pai, S. I. & Westra, W. H. Molecular pathology of head and neck cancer: implications for diagnosis, prognosis, and treatment. *Annu. Rev. Pathol.* **4**, 49–70 (2009).
104. Pai, S. I. et al. Comparative analysis of the phase III clinical trials of anti-PD1 monotherapy in head and neck squamous cell carcinoma patients (CheckMate 141 and KEYNOTE 040). *J. Immunother. Cancer* **7**, 96 (2019).
105. Carney, B. et al. Target engagement imaging of PARP inhibitors in small-cell lung cancer. *Nat. Commun.* **9**, 176 (2018).
106. Kossatz, S. et al. Detection and delineation of oral cancer with a PARP1 targeted optical imaging agent. *Sci. Rep.* **6**, 21371 (2016).
107. Kossatz, S., Weber, W. & Reiner, T. Detection and delineation of oral cancer with a PARP1-targeted optical imaging agent. *Mol. Imaging* **16**, 1536012117723786 (2017).
108. Kossatz, S. et al. PARP1 as a biomarker for early detection and intraoperative tumor delineation in epithelial cancers–first-in-human results. Preprint at *bioRxiv* https://doi.org/10.1101/663385 (2019).
109. Couzin-Frankel, J. Medicine contends with how to use artificial intelligence. *Science* **364**, 1119–1120 (2019).
110. Goodsaid, F. M. The labyrinth of product development and regulatory approvals in liquid biopsy diagnostics. *Clin. Transl. Sci.* **12**, 431–439 (2019).
111. Pantanowitz, L. et al. Twenty years of digital pathology: an overview of the road travelled, what is on the horizon, and the emergence of vendor-neutral archives. *J. Pathol. Inform.* **9**, 40 (2018).
112. Kozma, P., Kehl, F., Ehrentreich-Förster, E., Stamm, C. & Bier, F. F. Integrated planar optical waveguide interferometer biosensors: a comparative review. *Biosens. Bioelectron.* **58**, 287–307 (2014).
113. He, Z., Lee, Y. H., Chanda, D. & Wu, S. T. Adaptive liquid crystal microlens array enabled by two-photon polymerization. *Opt. Express* **26**, 21184–21193 (2018).
114. Kuznetsov, A. I. et al. Laser-induced transfer of metallic nanodroplets for plasmonics and metamaterial applications. *J. Opt. Soc. Am. B* **26**, B130–B138 (2009).
115. Lin, R. J. et al. Achromatic metalens array for full-colour light-field imaging. *Nat. Nanotechnol.* **14**, 227–231 (2019).
116. Wolfer, T., Bollgruen, P., Mager, D., Overmeyer, L. & Korvink, J. G. Printing and preparation of integrated optical waveguides for optronic sensor networks. *Mechatronics* **34**, 119–127 (2016).
117. Hui, H. Y. L. et al. "Immuno-flowFISH" for the assessment of cytogenetic abnormalities in chronic lymphocytic leukemia. *Cytometry A* **95**, 521–533 (2019).
118. Mazzini, G. & Danova, M. Fluorochromes for DNA staining and quantitation. *Methods Mol. Biol.* **1560**, 239–259 (2017).
119. Ng, B. L., Fu, B., Graham, J., Hall, C. & Thompson, S. Chromosome analysis using benchtop flow analysers and high speed cell sorters. *Cytometry A* **95**, 323–331 (2019).
120. Smith, P. J., Darzynkiewicz, Z. & Errington, R. J. Nuclear cytometry and chromatin organization. *Cytometry A* **93**, 771–784 (2018).
121. Gupta, A. et al. Deep learning in image cytometry: a review. *Cytometry A* **95**, 366–380 (2019).
122. Jarrett, K., Kavukcuoglu, K., Ranzato, M. A. & LeCun, Y. in *IEEE 12th Int. Conf. Comput. Vis.* 2146–2153 (IEEE, 2009).
123. Nair, V. & Hinton, G. E. in *Proc. 27th Int. Conf. Mach. Learn.* 807–814 (2010).
124. Bridle, J. S. Training stochastic model recognition algorithms as networks can lead to maximum mutual information estimation of parameters. *Adv. Neural Inf. Process. Syst.* **2**, 211–217 (1990).
125. Zhou, Y. T. & Chellappa, R. in *IEEE Int. Conf. Neural Netw.* 71–78 (IEEE, 1988).
126. Srivastava, N., Hinton, G., Krizhevsky, A., Sutskever, I. & Salakhutdinov, R. Dropout: a simple way to prevent neural networks from overfitting. *J. Mach. Learn. Res.* **15**, 1929–1958 (2014).
127. Yosinski, J., Clune, J., Bengio, Y. & Lipson, H. How transferable are features in deep neural networks? *Adv. Neural Inf. Process. Syst.* **27**, 3320–3328 (2014).

Acknowledgements

The authors acknowledge extensive discussions with L. K. Chin, J. Min, J. Oh, H. Im, T. Rainer and J. Carlson, and thank C. Landeros for discussions on machine learning and K. Joyes for editing the manuscript. The authors are indebted to J. Higgins and C. Vinegoni for the critical review of the manuscript. The authors are supported by the following grants: NIH- UH3 CA202637, NIH- U01CA206997, NIH- R01CA204019 and NIH- R01CA206890 (R.W.); NIH- R01CA229777, NIH- U01CA233360, DoD- W81XWH1910199, DoD- W81XWH1910194 and MGH Scholar Fund (H.L.).

Author contributions

Both authors contributed equally to the preparation of this review.

Competing interests

R.W. declares that he has received consultancy payments from Tarveda Pharmaceuticals, Mode RNA, Alivio Therapeutics and Accure Health, and that he is a shareholder of T2 Biosystems, Lumicell, Accure Health and Aikili Biosystems. H.L. declares that he has received consultancy payments from Exosome Diagnostics and Accure Health, and that he is a shareholder of Accure Health and Aikili Biosystems. Patents: all patents associated with R.W. and H.L. have been assigned to and handled by Massachusetts General Hospital.

Publisher's note

Springer Nature remains neutral with regard to jurisdictional claims in published maps and institutional affiliations.

Supplementary information

Supplementary information is available for this paper at https://doi.org/10.1038/s41578-020-0180-6.